The Science and Technology Journal of AWE

Discovery 17

September 2008

Discovery17 • The Science and Technology Journal of AWE

AWE is the trading name of AWE plc
Registered office: Aldermaston Reading Berkshire RG7 4PR
Registered number 3664571

The Science & Technology Journal of AWE • Issue 17 • September 2008

Discovery

Contents

cover image
Bonner spheres

Designed & produced by AWE Media Group
Printed in England by CDS
Printed on 9 Lives

17

It is my pleasure to introduce the latest edition of Discovery, the science and technology journal of AWE. As Editor perhaps I should start out by saying that this is now the second edition containing the updated layout.

Our aim in making changes was simply to freshen up the design – it has been largely untouched since the journal was launched some eight years ago. We have received a significant number of positive comments on the changes and will continue to seek areas of enhancement and introduce further changes as we move forward.

The original aim of Discovery was to provide a window through which the diversity and quality of science and technology at AWE could be displayed. Since the first edition was published in March 2000 we have endeavoured to give a broad and detailed flavour of the work at AWE that underpins nuclear deterrence. We have covered the major platforms of physics, chemistry, materials and engineering, and increasingly addressed the expanding area of simulation and modelling to add a further dimension to the traditional approach of theory and experiment. During the last eight years we have covered a broad range of topics and have continued to expand our distribution - Discovery is widely circulated both within AWE, the local community, wider within UK industry and universities as well as being sent overseas.

Recent editions have commented on the exciting times at AWE following the announcement by the Government of the decision to renew the UK's minimum deterrent, with the White Paper published in December 2006 and the debate and vote in Parliament in March 2007. In parallel with this has been the significant investment in both people and facilities at AWE to underpin its role into the future. As we go to press, the new Orion Laser dominates the western edge of the Aldermaston site with the installed equipment phase now well underway. At our Burghfield site we have recently opened a major refurbished facility handling non-metallic materials and have embarked on a major demolition programme to remove a number of old buildings to make room for new facilities.

Issue 17 of Discovery contains articles on solid waste assaying, fibre optic sensors, neutron spectrometry, plasma opacity and high strain rate spall effects. In addition we have included a summary of the internal Science, Engineering and Technology (SET) awards that were presented to AWE staff earlier this year.

I hope you enjoy reading this issue – it is a showcase for AWE and the vital contribution it makes to strategic defence.

Dr David Glue
Director Stockpile Management

HELEN High Strain–Rate Spall Experiment

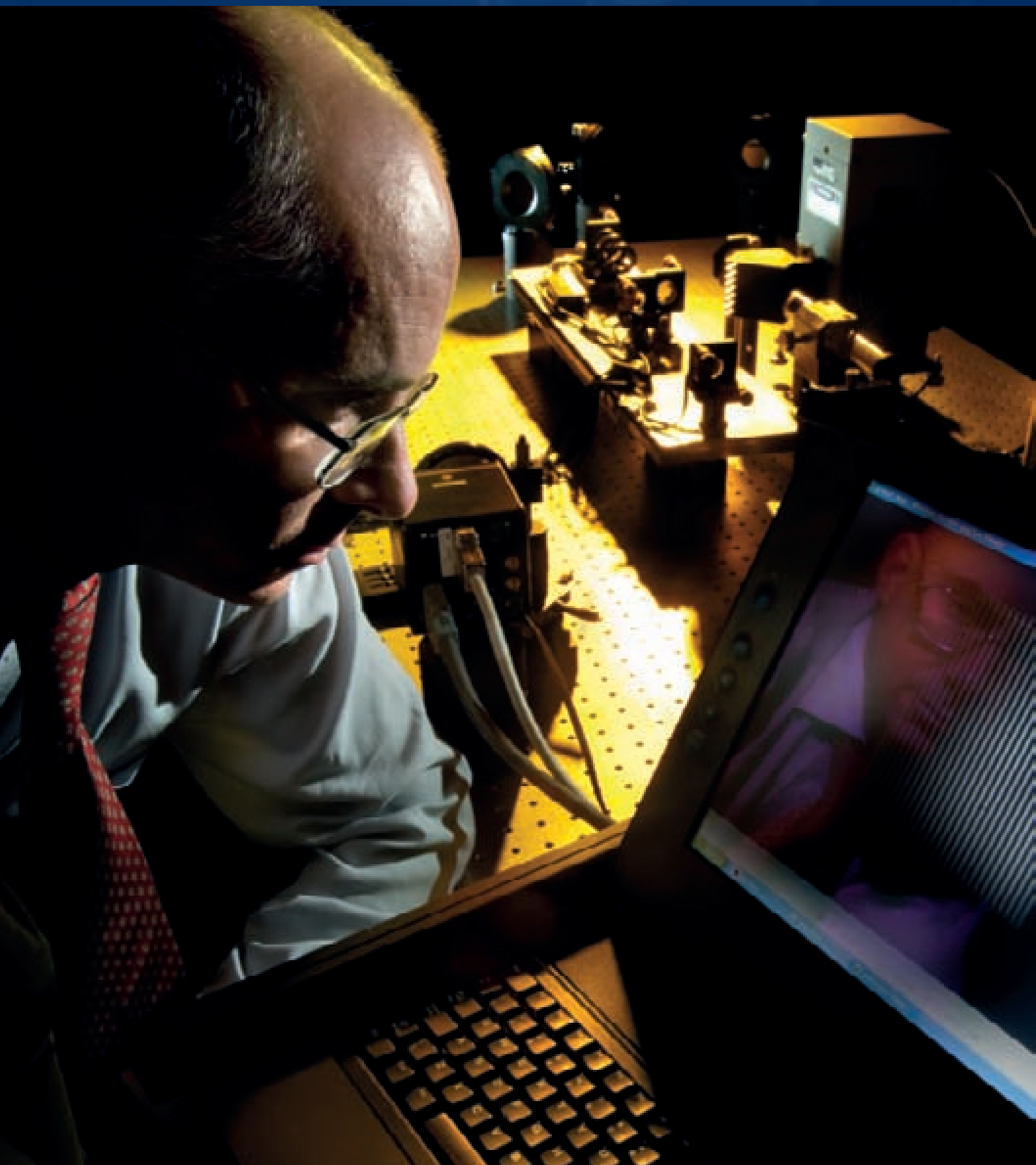

Laser irradiation of the front of an aluminium target produces a shock wave. As this propagates through the target it is overtaken by the rarefaction launched when the laser turns off, producing a triangular pulse with a near-instantaneous rise and fast, approximately linear, fall in pressure.

When the shock wave breaks out at the rear surface of the target a second rarefaction wave is produced, propagating back into the material. Superposition of these two rarefaction waves gives a net tension which increases with distance from the rear surface. If, at some distance away from the rear surface, this induced tension exceeds the strength of the material the target will break, or spall, and a layer is detached and flies away from the bulk of the target.

Measuring the surface velocity-time profile allows estimates of material strength, and provides data to fit parameters of material spall models. Imaging the spall measures the thickness of the spall layer to confirm values calculated both from simulations and from the velocity data. Figure 1 shows a schematic of the experimental set-up. Recovery either of the spall layer or the bulk of the target again confirms the spall layer thickness and provides metallurgical data to study spall mechanisms and effects of material structure such as grain size and orientation.

Spall experiments have been carried out on HELEN in the past to backlight spall layers and to use position-sensitive interferometry (both point and 1D spatially-resolving Michelson interferometers) to assess spall strength. Figure 2 shows example data. Our results showed a much higher spall-strength at intermediate rarefaction strain rates (fractional length change of the material divided by timescale) compared with data from Moshe *et al.* [1,2] (see Figure 3). Though laser-driven experiments have much higher strain rates than explosively or impact-driven ones, any model that can fit a wider range of strain rates is presumably more robust than one restricted to a limited range. Additionally, some of the targets were recovered (Figure 2c), allowing us to investigate the spall mechanism for aluminium. However, we have never succeeded in simultaneously measuring surface velocity, imaging the spall layer and recovering the sample.

The aims of these shots were to:

- Commission a new AWE VISAR (Velocity Interferometer System for Any Reflector). [3]
- Commission a new Heterodyne-Velocity Interferometer (Het-V, or Photon-Doppler Velocimeter (PDV)), and cross-check VISAR and Het-V results.
- Investigate spall in Al at strain rates from ~10^6 to $2x10^7$ s^{-1}.
- Backlight the spall layers.
- Recover targets for metallurgical examination, especially with reference to pre-shot Electron BackScatter Diffraction (EBSD) characterisation.

FIGURE 1

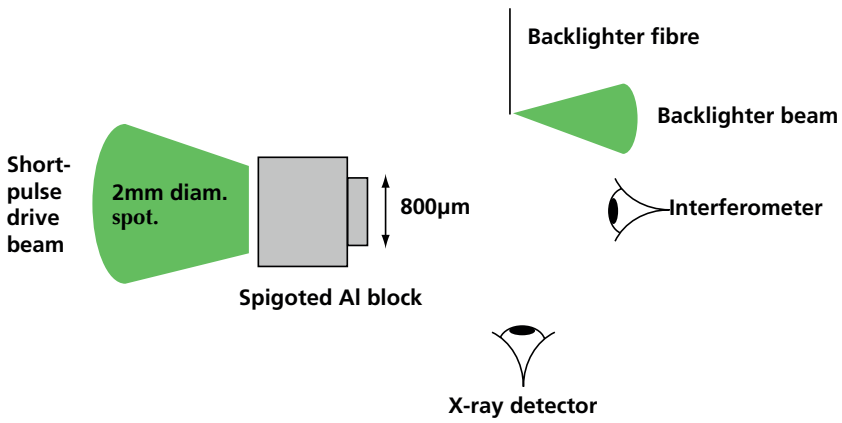

Schematic of spall experiment. The defocussed laser beam irradiates the front of an Al disc sample whose rear surface motion is then observed by velocity interferometry and side-on X-ray backlighting.

Experimental Design

The rarefaction strain rates are set by the attenuation of the triangular shock profile as it travels through the target. Simulations, using calculated pressures in Al for different laser energies, were done to find target thicknesses giving shock breakout pressures of the order of the spall strength, and the corresponding strain rates. Essentially strain rates were fixed by the decay of the shock, and so by target thickness, which in turn fixed the laser energies. The thinnest targets gave the highest strain rates (~$2x10^7$ s^{-1} for 50µm thickness and 500 Jcm^{-2} laser fluence) while the thickest targets gave the lowest (~$5x10^5$ s^{-1} for 2000 µm thickness and 2000 Jcm^{-2} laser fluence). (The 2000 µm targets were affected by lateral rarefactions so the actual strain rates would be lower than the 1D predictions.)

Targets

These were Al discs ~2.5mm in diameter and 50, 100, 250, 500 or 2000 µm thick. The 250 µm and thicker targets had 800µm diameter, 100 µm high spigots machined on the rear surfaces. It was hoped to use EBSD to characterise the rear surface grain size and orientation, but only two targets were done this way. Figure 4 shows a processed EBSD map of grain orientation.

The intention was to align the VISAR's streak camera slit along an identifiable line from this scan and correlate differences in shock breakout time, spall strength and mechanism, etc. with the EBSD data.

Experimental Set-up

The front faces of the targets were irradiated by the HELEN West beam through a 2 mm spot phase zone plate with additional ~4.5 mm defocus to give uniform drive. A 1ns square pulse was used, giving energies from 5 J to 200 J.

The VISAR looked normally at the rear (East) surface of the target through an f/3 focussing lens. A 45° turning mirror relayed probe-laser light into, and reflected light out of, the chamber to the North (see Figure 5). The probe was a ruby laser giving ~20 mJ in 150 ns pulses at 694 nm. The VISAR output was recorded on a streak camera at sweep speeds of 1 or 2 $ns.mm^{-1}$ (nominal); a 1392x1024 pixel CCD recorded the streaks. The VISAR superimposes two images of the target formed by different paths, one with a time delay provided by an étalon. Velocity is found from the changing phase difference between these paths due to the Doppler shifts of different target-surface velocities at different times. A VISAR is usually operated with a static fringe pattern, to simplify Fourier analysis, superimposed on the image by tilting a mirror within the VISAR.

The Het-V used a 1550 nm off-the-shelf telecommunications laser relayed to the target via a fibre optic. This was set to look at the target through the VISAR turning mirror and lens, and also with two dedicated shots where the probe was set close to the target.

FIGURE 2

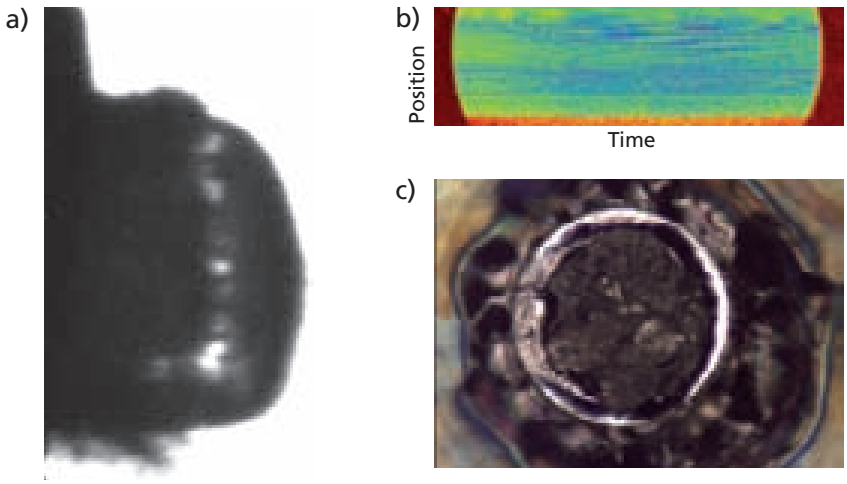

Earlier HELEN results: (a) Backlit side-on image of spall layer. (b) Line-imaging Michelson interferometer streak showing surface motion, differential shock breakout from base and spigot and lateral rarefactions. (c) Face-on photograph of recovered target showing material spalled from both base and spigot.

"The VISAR superimposes two images of the target formed by different paths, one with a time delay provided by an étalon."

FIGURE 3

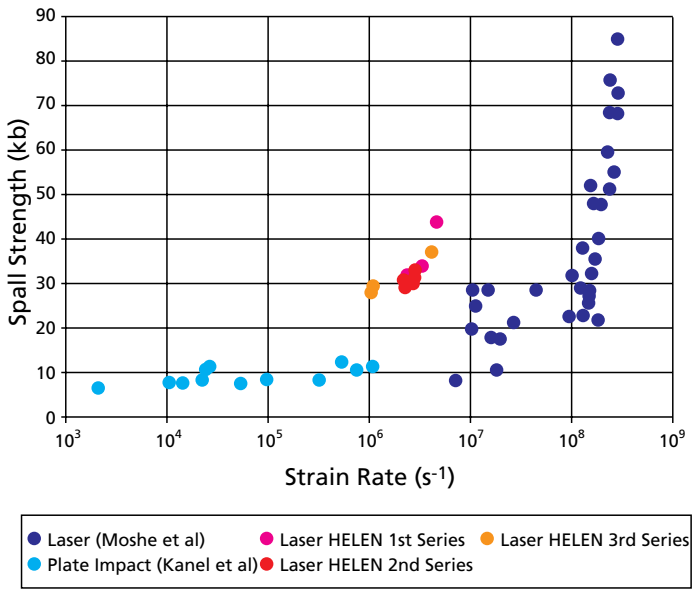

Plot of spall strength vs strain rate showing anomalously high HELEN strength results compared with data from Moshe et al. [1]

FIGURE 4

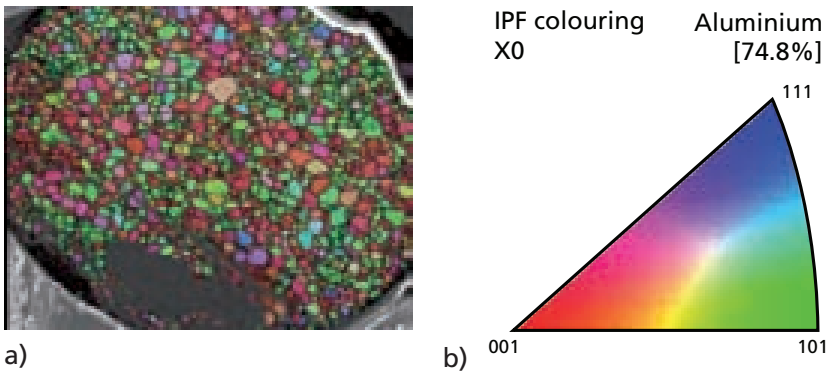

Processed EBSD scan of a target, (a) Grains are shown coloured acccording to their crystallographic orientation. Roughly speaking the (R,G,B) numbers of the colour at each point correspond with the extent to which the orientation is aligned with the major crystallographic planes, the {001}, {101} and {111} planes respectively, as shown on the key next to the scan (b).

Three different probe set-ups were used: *(i)* a flat fibre end (15dB reflectance) with a GRaded INdex (GRIN) lens 380±20 mm from target; *(ii)* a dedicated probe assembly with a 240 mm focal length lens (40dB); and *(iii)* a flat fibre (15dB) 1–2 mm from target. Data were recorded on a 20 Gsamples s^{-1} (effectively 7 GHz) digitising storage scope. Target velocity is found from the beat frequency between light reflected from the probe end and the Doppler-shifted light from the target.

The original plan to X-ray backlight targets used pinhole-apertured Ti foil targets but it was decided during the experiment to try proton backlighting. A 10 µm Au foil irradiated by a 1ps, 50 J, 1054 nm pulse was used to generate protons which were recorded on a stack of ~15 sheets of radiochromic film at ~10x magnification.

No specific arrangements were made to recover targets. Instead we relied on the bulk of the target remaining on the mount, as they had during the previous spall shot series. In the event, none did; but about 20 targets were recovered by looking in the chamber post-shot, and most of these could be matched reliably to that particular shot.

Results

About 40 shots were fired on test targets and about six of each of the five thicknesses (strain rates). Figure 6 shows VISAR data for two example shots. Around 20 targets were recovered, showing the full range of behaviours from incipient spall through actual spall to near complete destruction of the target.

The Het-V did not give any meaningful data, nor did the two attempts at proton backlighting.

We are beginning to analyse VISAR data. The streaks are analysed column-by-column (time-by-time): each column is Fourier-transformed and the mode corresponding to the imposed fringe pattern identified, shifted to the mode-zero position, filtered with a narrow-band mask to remove lower-mode spatial non-uniformites and high-frequency noise and inverse-transformed. The phase of this complex result is obtained from $\tan^{-1}$(Imaginary part/Real part) and velocity is given by the phase multiplied by the VISAR velocity-per-fringe (VPF).[3] Discontinuities of multiples of 2π in phase may need to be removed, arising from VISAR fringe jumps of more than one fringe, which are indistinguishable; and multiples of π from the arctangent function being bounded between $\pm\pi/2$. The latter can be done more or less automatically but the former needs to be done by eye with reference to the expected peak velocities. (It is usual to use two VISARs with different VPFs to discriminate unambiguously between possible velocities.)

FIGURE 5

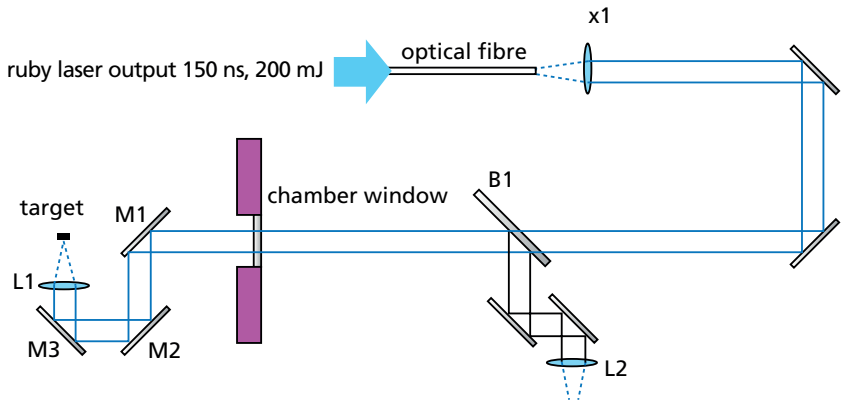

Schematic of VISAR set-up (plan view). The ruby probe laser is fed in from the top of this diagram. The reflected light is imaged onto the VISAR and then the streak camera via beamsplitter B1 and lens L2.

"The simulation for the nominal laser energy showed very good agreement in breakout time, but a ~20% difference in surface jump-off velocity."

Analysed velocity for shot 3806, a 500 μm target, is compared with simulation in Figure 7. The simulation for the nominal laser energy showed very good agreement in breakout time, but a ~20% difference in surface jump-off velocity. The simulation plotted is scaled in laser energy to match the jump-off velocity and shifted in time by ~3 ns to match the breakout.

These discrepancies were seen in previous series and may be due to errors in laser energy (which is measured less accurately at low values such as these shots) or VISAR timing; they may also be due to the aluminium equation of state and strength used by the code. The intention is to match the experimental velocity profile by varying the spall model's parameters. The expected elastic precursor is not seen in the data. However, the characteristic spall signature of pull-back (falling velocity) followed by a jump at spall is clear, and is followed by a further reverberation of the shock within the spall layer. The velocity difference Δu between peak and first minimum gives an estimate of spall strength σ from

1 $$\sigma = \tfrac{1}{2}.\rho_0.c_0.\Delta u,$$

where ρ_0 is the solid density and c_0 the bulk sound speed. The corresponding time difference Δt gives the spall layer thickness

2 $$T = \tfrac{1}{2}.c_L.\Delta t,$$

where c_L is longitudinal sound speed, and the strain rate is:

3 $$d\varepsilon/dt = \tfrac{1}{2}.c_0.(\Delta u/\Delta t)$$

FIGURE 6

a)

b)

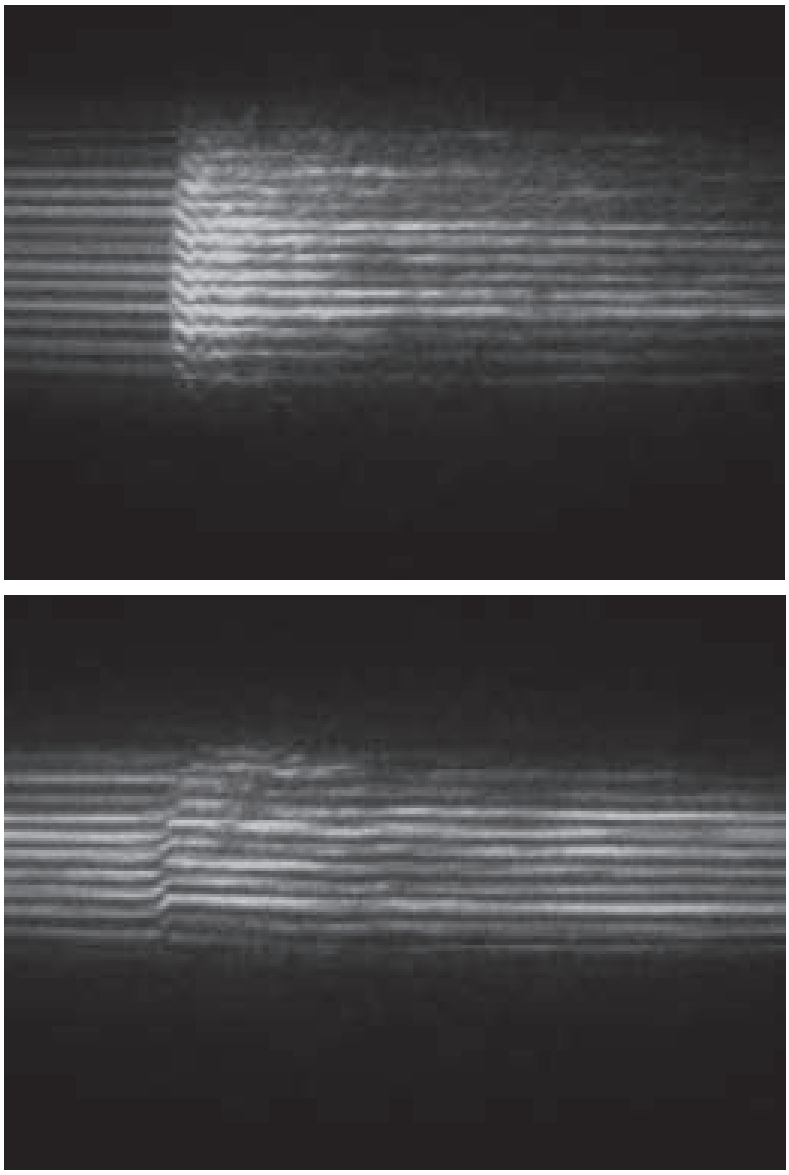

(a) VISAR data for shot 3805, a 50 μ thick target, and (b) data for shot 3806, a 500 μ thick target.

"The expected elastic precursor is not seen in the data. However, the characteristic spall signature of pull-back (falling velocity) followed by a jump at spall is clear . . ."

FIGURE 7

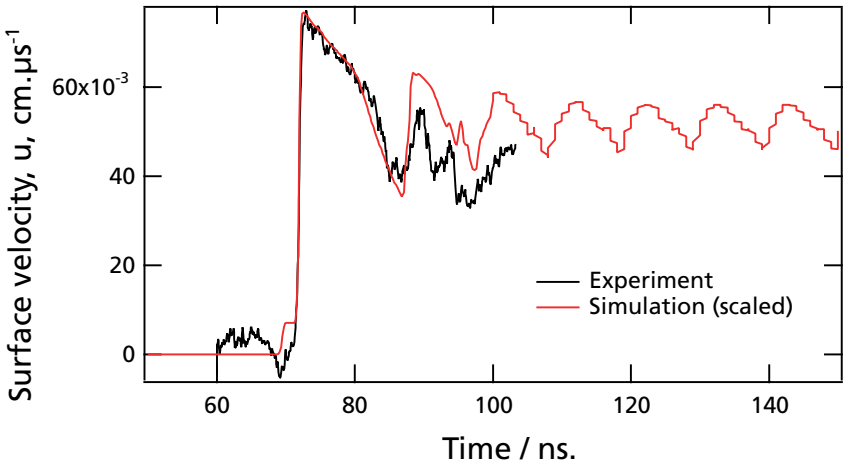

Analysed velocity-time for shot 3806, a 500 µ thick target, compared with simulation based on scaled laser energy to match the post-shock jump-off velocity and time-shifted to match breakout. The data show the jump in velocity on shock breakout, pullback (including a change in slope indicative of an elastic-plastic transition), jump in velocity on spall, and a further reverberation of the wave within the spall layer.

FIGURE 8

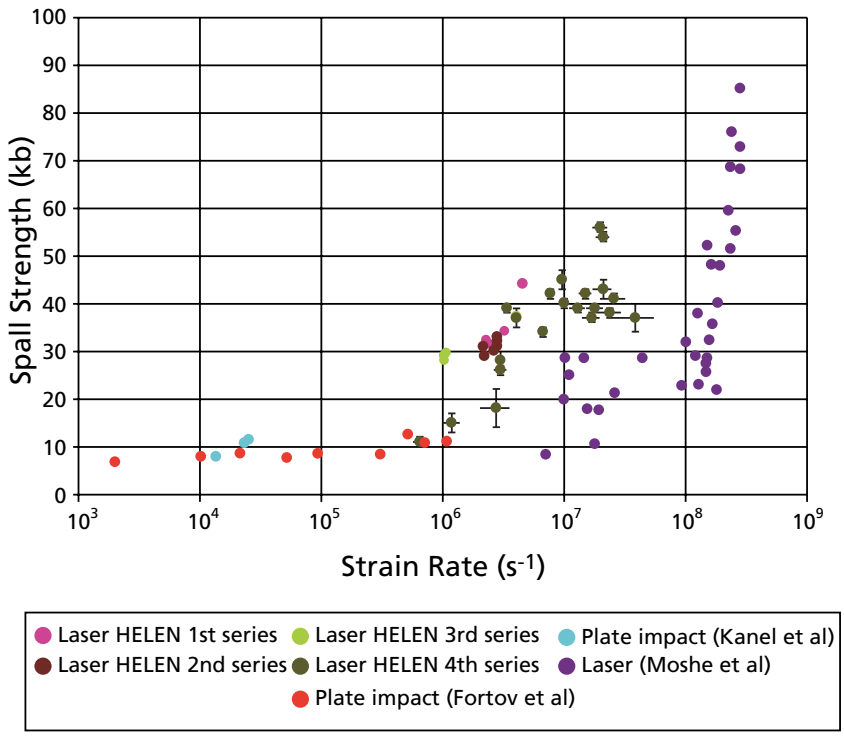

Preliminary spall strength vs strain rate from velocity-time profiles. Earlier results as in Figure 3.

Figure 8 plots a preliminary analysis of spall strength against strain rate.
The velocity-time profile also shows the change from elastic to plastic behaviour as the change in slope of the pullback.

The recovered targets have yet to be analysed by SEM imaging.

Two shots were fired using proton backlighting but there is no sign of an identifiable target, possibly due to a weak and unfocussed proton beam from poor laser beam quality.

Summary and Conclusions

The VISAR was successfully fielded for the first time and used to take data for ~35 shots. The Het-V did not give any useful data but the cause is not known.

Two attempts at imaging the spall layer using protons were unsuccessful, probably due to poor laser beam quality.

About 20 targets have been recovered and are awaiting metallurgical examination. One of these has pre-shot EBSD data and so spall metallurgy and VISAR data can be related to the target crystal structure.

Acknowledgements

The following also helped write this article:

J.Turner (simulations).
H.Davies (VISAR).
E.Price (MET-V).
S.James (experimental assistance).
N.Park (theory and metallurgy).

References

1 E. Moshe, S. Eliezer, Z. Henis *et al.*, Appl. Phys. Lett. 76(12), March 2000

2 G. I. Kanel, S. V. Razorenov, A. V. Utkin and K. Baumung, Shock Wave Profile Data, Scientific Association IVTAN of Russian Academy of Sciences (1996)

3 P. M. Celliers, D. K. Bradley, G. W. Collins *et al.*, Rev. Sci. Inst. 75(11), p4916 (2004)

AUTHOR PROFILE

S.Rothman
can be contacted on e-mail:
steve.rothman@awe.co.uk

After graduating from the University of Cambridge in 1985 Steve started work in the Radiation Physics division of AWE. He has worked on a variety of experiments using the HELEN laser, the NOVA laser at the Lawrence Livermore National Laboratory (LLNL) in California, including a ten-month stay there in 1991, at the laser facilities at Los Alamos, LLE (University of Rochester), and at the "Z" pulsed-power machine at Sandia Laboratory. Areas addressed have included the implosion of cylinders to investigate their hydrodynamic stability; the acceleration of planar foils; the propagation of shocks and their interaction with embedded particles and obstacles and, currently, measurements of equation-of-state of metals and plastics at multi Mbar pressures. In particular these last experiments have involved high-accuracy shock-wave measurements and the development of techniques to analyse shockless compressions.

Advances in Solid Radioactive Waste Assay Capability

Many forms of radioactive waste and authorised discharges are assayed by a variety of radiometric (i.e. radiation-based measurement) techniques. These techniques involve the detection of one or more of the inherent radiation types: alpha particles (α), beta-rays (β), gamma-rays (γ) or neutrons (n), emitted by the radioactive material during its natural decay.

Any decision regarding the final destination for such wastes is dependent upon the activity level assigned to such wastes. The confident sentencing of radioactive wastes is therefore strongly correlated with the assay approach, particularly with respect to achieving the desired assay sensitivity, which directly impacts the detection limit, and in determining the total measurement uncertainty. At the other end of the scale, there is also a need to provide assurance that the total activity, say within a waste drum, does not exceed the defined limit set by safety considerations.

In the case of solid radioactive drummed wastes containing predominantly plutonium (Pu) or uranium (U) of a variety of isotopic compositions, the measurement is essentially restricted to the detection of emitted gamma-rays (for both Pu and U) and neutrons (realistically for Pu only, given the correspondingly low spontaneous fission decay rates for isotopes of U). The assay process itself is termed non-destructive, in that the waste remains in its original prepared state and the chosen assay technique samples the emitted radiation remotely from the undisturbed waste container. The abbreviation NDA is commonly applied to the overall non-destructive assay process.

The NDA measurement challenge

The interpretation of the measured gamma-ray and neutron radiation signatures emanating from a waste container must take account of various factors which can perturb the emitted radiation. These relate to the density and degree of homogeneity or otherwise of the waste matrix, the spatial distribution of the Pu

FIGURE 1

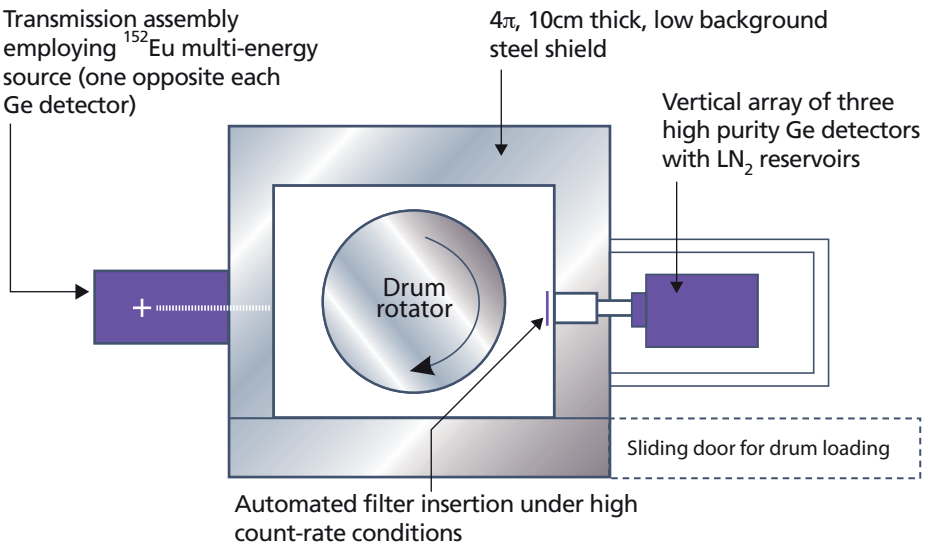

A schematic plan view of the AQ2 gamma-ray assay system indicating the principle features, i.e. location of detectors and transmission sources relative to the waste drum under assay within its shielded enclosure.

or U within the drum, the degree to which the Pu or U is lumped, and the extent to which radiations emitted by Pu or U interact with the waste matrix to produce other characteristic radiations that may help or hinder the assay process. Material lumpiness will provide a degree of self-shielding to the emission of gamma-rays and is more prevalent the lower the energy of the gamma-ray. For Pu and U a lump broadly equates to a material thickness of the order of one to a few mm. On the other hand, the neutron output from lumped Pu will be amplified by neutron multiplication effects. The attenuating properties of the waste matrix and its container can be assessed for both gamma-rays and neutrons by using an external transmission source. A detailed discussion of the NDA challenge presented by fissile materials, in particular the determination of these correction terms necessary to accurately relate the measured radiation output to the material quantity, was previously published in issue 2 of Discovery.[1]

Advances in waste assay instrumentation

In late 2006 an integrated drum assay suite was commissioned and is now in operational service. The purpose of this suite which comprises a multi-detector high-resolution gamma-ray detection system (termed the AQ2) and a high efficiency neutron counter (HENC) with improved (i.e. lower) detection limits compared to previous generations of similar assay equipment, is to:

- Re-assess stored, legacy 200 l waste drums to determine those that are UK intermediate level waste (ILW) and those that are low level waste (LLW). The boundary or sentencing threshold for UK LLW is an α activity content ≤ 4 GBqte^{-1}.

- Determine that fraction of the re-assessed UK LLW drums which have the potential to be consigned to the National Low Level Waste Repository near Drigg in Cumbria. Here the requirement is to meet a more challenging 0.1 GBqte^{-1} limit.

- Provide assurance that stored drums do not exceed any safety-derived limit; e.g. mass limits for fissile materials (Pu and enriched U) that may be stored within a drum set by criticality-safety considerations.

- Ensure a quality record of the complete inventory of radionuclides is maintained to permit storage in any future UK waste repository. In this manner, future waste processing activities (e.g. super-compaction of 200 l drums and final placement of a number of these within 500 l grouted over-pack drums) will not demand additional NDA.

The feedstock to the waste assay suite covers an extremely wide range of waste matrix types. They vary from coveralls and other low density homogeneous wastes through to discrete high density metallic items, forming a heterogeneous matrix alongside lower density infill materials. The associated fissile material contents range from typically mg quantities to many 10s of grams and above. The penetrability of neutrons arising from the spontaneous fission of even mass Pu isotopes through dense metallic materials makes them ideally suited as a complementary signature to gamma-rays (which suffer significant attenuation in such materials) to enable

"The penetrability of neutrons arising from the spontaneous fission of even mass Pu isotopes through dense metallic materials makes them ideally suited as a complementary signature to gamma-rays . . ."

a more accurate assay to be undertaken. Whilst the HENC therefore is specific to Pu mass determination, the AQ2 provides a comprehensive determination of the activities of all gamma-ray emitting radionuclides. This wide dynamic operating regime, coupled with a demanding drum throughput requirement, necessarily leads to an automated assay and data analysis approach in which operator input is minimal.

Figures 1 and 2 show simple schematics of the assay approaches employed by the AQ2 gamma-ray system and the HENC neutron counter respectively. Figure 3 shows the installed integrated system; a drum conveyor system links the two measurement chambers.

Improvements to assay functionality

The procurement and commissioning process for this drum assay suite, commonly referred to as SILWAS (solid intermediate level waste assay system) involved the design and incorporation of advanced assay functionality in order to address a number of measurement challenges posed by the wide dynamic assay range (i.e. from mg to ~100 g of fissile material per 200 l drum), and the requirement to quantify realistic measurement uncertainties and thereby improve confidence in the sentencing capability of the system. The latter involved a detailed examination of the aforementioned correction factors, including an assessment of their correlation.

These improved assay features, specified by the NDA Technical Authority, were implemented by the SILWAS supplier, Canberra UK, and involved close collaboration between both parties in testing the validity of the software-driven operational and analysis code enhancements. The benefits of forging and maintaining this strong customer-supplier link were the evolution

FIGURE 2

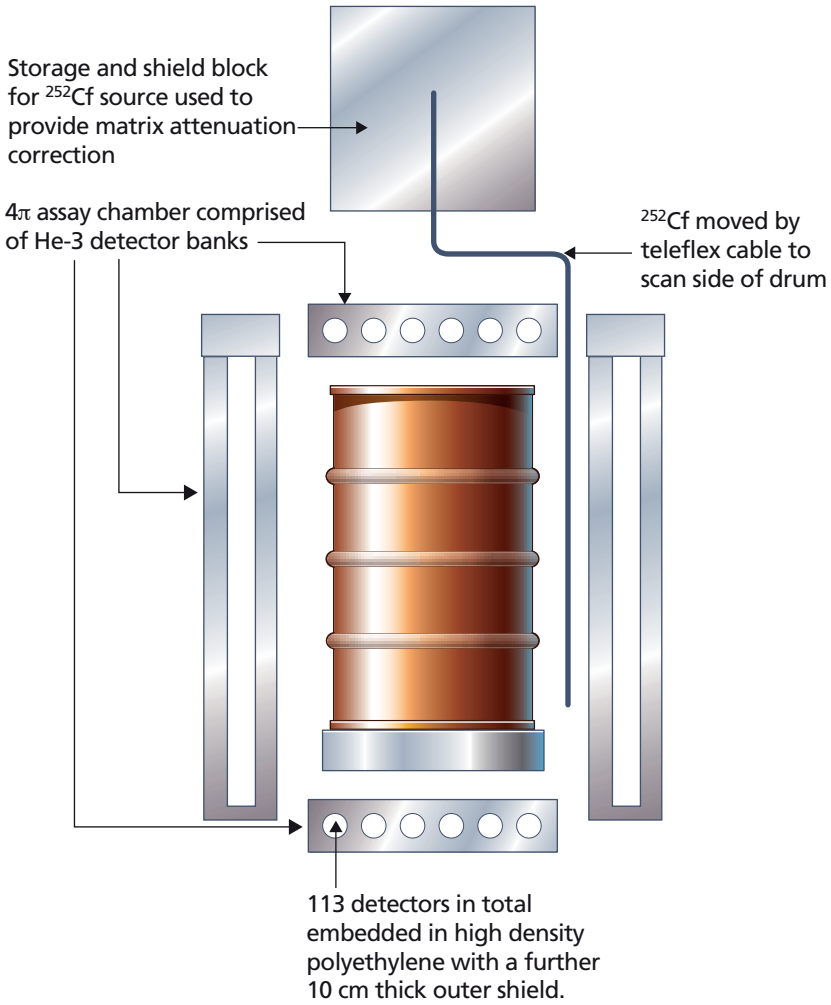

A schematic of the HENC neutron assay system indicating the principle features, i.e. location of detectors relative to the waste drum under assay within its neutron moderating enclosure.

FIGURE 3

The installed SILWAS system showing the conveyor linkage between the two assay elements, the AQ2 and the HENC. Figure shows a drum inside the HENC component of SILWAS.

of a mutual understanding of the technical challenge presented by each improvement, a consensus approach to the formulation of each solution, and optimised validation testing.

The assay features bespoke to the AWE SILWAS, and their status, are as follows:

- Improved Pu isotopic and U enrichment determination through the use of a proprietary gamma-ray analysis package developed for International Safeguards. A separate algorithm has also been developed which can robustly (i.e. independent of the material thickness) attribute U to one of a number of pre-defined enrichment categories. This algorithm has been validated under the most severe gamma-ray self-attenuation conditions and takes over from the proprietary software analysis package if the data collected (proportional to the amount of U material present) are insufficient for a statistically meaningful isotopic analysis.

- Extended gamma-ray analysis capability to determine the presence of (α,n) interactions in the low atomic number (Z) elements present within the

> "The AQ2 system flags the presence of gamma-rays associated with α particle interactions in low Z materials, and this flag is used in the SILWAS decision tree"

waste matrix. For example, Be and F in intimate contact with Pu are prolific emitters of neutrons, and add to those neutrons generated by the spontaneous fission of Pu. However, these elements also emit characteristic gamma-ray signatures at 4.4 MeV and 1274 keV respectively, which can be used to infer the presence of such reactions. Such (α,n) neutrons can, under some conditions, give rise to further induced fission, which, if uncorrected for, can lead to an overestimate of the Pu content of the waste as determined by the HENC. The AQ2 system flags the presence of gamma-rays associated with α particle interactions in low Z materials. This flag is used in the SILWAS decision tree to weight the HENC-derived Pu assay result accordingly when it comes to deducing the most likely mass or equivalent activity within the drum based on the independent determinations made by the HENC and AQ2.

- Implementation of a revised analysis methodology for determining Pu and U self-absorption corrections. A set of equations linking true mass to apparent mass as a function of gamma-ray energy has been derived from a database of numerically modelled gamma-ray emission rates for an extensive range of fissile material lump sizes.
  In the case of U self-absorption, the correction first calls for the material to be allocated within one of the aforementioned enrichment categories. In some instances the crude gamma-ray imaging capability of the AQ2 indicates the presence of a single or small number of U lumps, but there is no measurable ^{238}U gamma-ray signature (at 1001 keV) from which to deduce the corresponding enrichment category. In these cases the magnitude of the ^{235}U 185 keV gamma-ray line alone is used within an empirically-based expression to provide an upper bound to the size (mass) of the U lump(s).

- Comprehensive determination and reporting of a realistic total measurement uncertainty (TMU) associated with each detected radionuclide in a format that distinguishes statistical from systematic contributions to the TMU.
  In addition to the standard statistical measurement uncertainties and those uncertainties in the activities of those radioactive standards used to characterise the AQ2 and HENC systems, the TMU algorithm contains contributions from:
  - Pu and U mass measurement uncertainties as propagated through the new gamma-ray self-absorption and, for U only, lump correction analyses,
  - Systematic uncertainties arising from non-uniform matrix-source distribution effects in both the AQ2 and HENC systems,
  - Isotopic ratio uncertainties,
  - Uncertainty in the neutron multiplication as determined by the HENC system; lumped Pu may well exhibit greater than unity neutron multiplication.

- Utilisation, where the Pu mass is sufficiently large, of higher order correlated neutron events to determine, and correct for, the effective neutron multiplication of the Pu-bearing waste.

- Implementation on the AQ2 of an automated drum type identification routine. This routine is necessary to make suitable corrections to the detected radiation signal for any attenuation caused by the drum itself or any other liner within the drum. This novel feature is based on the development of an empirical database of gamma-ray transmission information for each type of 200 l drum (including variants of inner waste liner) that are to be subject to the SILWAS assay process. The database examines transmission data as a function of gamma-ray energy in the topmost, i.e. lid, region of each drum, where there is minimal likely interference by the actual waste constituents.

TABLE 1

	AQ2		SGS	
Radionuclide	Soft waste	Hard waste	Soft waste	Hard waste
^{239}Pu (g)	~ 0.005	~ 0.009	~ 0.075	~ 0.115
^{235}U (g)	~ 0.003	~ 0.011	~ 0.035	~ 0.060
^{238}U (g)	~ 3.3	~4.7	~ 40	~ 55

Order of magnitude Detection limit (DL) values for the AQ2 and existing SGS gamma-ray detection based assay systems given their pre-determined assay times (including background determination) and typical background rates.

TABLE 2

	HENC		N94 PNCC	
Radionuclide	Soft waste	Hard waste	Soft waste	Hard waste
$^{240}Pu_{eff}$ (mg)	~ 1.6	~ 3.4	~ 10 -15	~ 15 – 25

Order of magnitude DL values for the HENC and existing N94 PNCC neutron detection based assay systems given their pre-determined assay times (including background determination) and typical background rates.

"The database examines transmission data as a function of gamma-ray energy in the topmost, i.e. lid, region of each drum, where there is minimal likely interference"

Summary

The assay functionality enhancements embedded in SILWAS yield improved confidence in waste sentencing and compliance with safety-derived fissile material limits for drummed wastes through a rigorous determination of the individual components of total measurement uncertainty. The actual design features of the AQ2 and HENC that comprise the SILWAS, in particular their methods of reducing background radiation interference effects (through application of shielding in the case of the AQ2 and data reduction algorithms that remove time-correlated cosmic-induced neutron events for the HENC) lead also to significant improvements in detection limit (DL) performance.

The quantified benefits in DL performance brought about by the investment in SILWAS are summarised in Tables 1 and 2 in which DL performance figures for the AQ2 and HENC are compared against forerunner equivalent assay systems, the drum-scale segmented gamma-ray scanner (SGS) and N94 passive neutron coincidence counter (PNCC) respectively.

DL figures are quoted for two typical waste matrix types; soft (PVC, polyethylene, rubber, and cellulose materials) at a density of ~ 0.1-0.25 g cm^{-3} and hard (various metals, glass and perspex) at a density of ~ 0.5 - 2 g cm^{-3}. The information contained in the tables is predominantly taken from a range of Acceptance Test documentation, but some use is made of manufacturers' data sheets and operational experience. The SILWAS system has a crucial role to play in the continued safe management of radioactive wastes.

References:

1. M Harker, "Non-Destructive Assay", Discovery Issue 2, p 46-51, (2001)

AUTHOR PROFILE

S.Holloway can be contacted on e-mail: steve.holloway@awe.co.uk

Steve Holloway • Steve majored in physics at Birmingham University. He gained his DIC and PhD from Imperial College under the Public Research Institute Scheme for experimental research conducted at AERE Harwell and the Ascot Reactor Centre in the field of low-energy nuclear physics, specifically the determination of the nuclear decay schemes of a number of actinide elements. Following a period of further nuclear physics postdoctoral research at Harwell Steve joined AWE in 1983. His career at AWE has focused predominantly on the development and application of radiometric techniques to the assay of fissile material at all stages of the nuclear weapon lifecycle. He is currently the Group Leader of the Non-Destructive Assay team within the Materials & Measurement Sciences Division.

Development and Application of Optical Fibre Sensors for use in Engineering trials

The aim of this article is to present an overview of the development of a fibre optic distance sensor (FODS). The project spanned a range of disciplines from research into the fundamental physics of the sensor to the development of a robust, engineered system that could be deployed in a trial assembly containing explosives.

The solution required concurrent research and development activities across multiple components which required differing levels of integration. These components had both complex internal interfaces and external constraints. Therefore, taking a systems approach became integral to achieving a successful outcome. An overriding project philosophy was to use well developed industrial technology, referred to as 'commercial off the shelf' (COTS) technology. In some cases this technology had to be modified and integrated. Only when absolutely necessary was fundamental research and development conducted.

The Trial

The primary aim of the trial is to measure the movement of an explosive component housed within a test assembly. The explosive component surrounds a central component and inner transparent polymer layer. This in turn is surrounded by an outer transparent polymer layer. The assembly is then encased within a sealed metallic container, Figure 1. The assembly is subjected to thermal and mechanical environmental conditions that result in the deformation of the compliant explosive, and may also lead to the formation of an air layer between the explosive component and transparent polymer layer. Intrusion into the system must be minimised to ensure that any data collected are representative of the system. Due to the presence of explosives, there should be no electrically conducting paths to the test assembly.

The trial consists of two distinct environmental testing phases. Initially the test assembly will be temperature cycled, between 20 and 30 °C. This procedure will be carried out in a thermal chamber over a period of three months. The second phase of the trial presents a greater degree of technical challenge. In order to simulate selected environments, the test assembly will be loaded onto a centrifuge and accelerated to around 200 gn for approximately two minutes. Due to constraints imposed by the test facility, it was necessary to locate all instrumentation on the centrifuge arm for this phase. The requirement is to measure the distance between the container and the compliant component with a measurement uncertainty of ± 10 µm. If air layers form, these must be detected and, if possible, should also be measured with an uncertainty of ± 10 µm. In order to imagine the scale of this uncertainty, a typical human hair and red blood cell are 80 µm and 8 µm in diameter respectively.

Following analysis of the problem, it was evident that an integrated suite of sensors, based on the general principles of fibre optic sensing, offered a number of key advantages for the trial.

FIGURE 1

A section of the test assembly, showing the probe configurations.

FIGURE 2

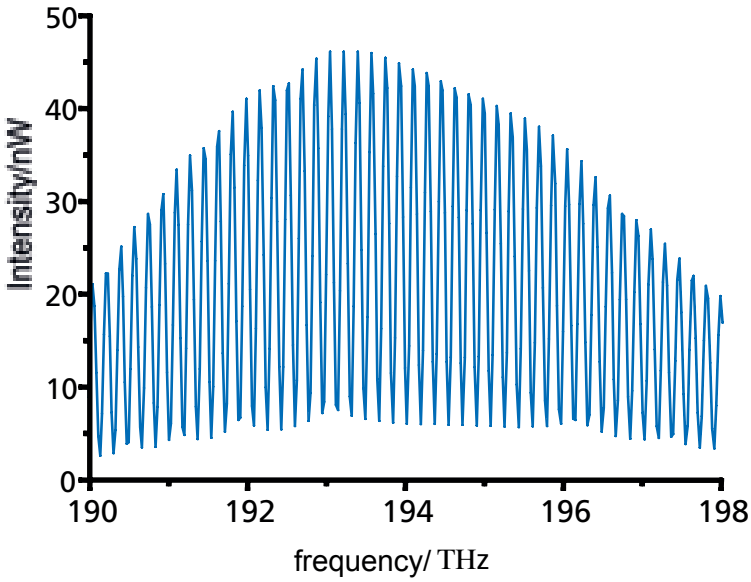

Typical interference pattern showing detail of the sinusoidal fringes.

These were minimisation of intrusion due to their small physical size; satisfying explosive safety regulations by eliminating the electromagnetic pathway through the sealed outer container; and the integration of distance and temperature sensors within the same common instrumentation, signal demodulation and processing system.

Fibre optic sensing is based on the principle that a parameter of the light guided by the fibre, for example its intensity, phase, wavelength or polarisation state, changes when subjected to an external influence such as temperature, pressure, or strain. Many companies presently offer COTS sensors using this principle.

Interferometry

Interference is observed when light, usually from the same source, travels along different paths to some remote point where it is detected. At the point of detection, light and dark bands, known as interference fringes, will occur due to the superposition of waves. By exploiting this phenomenon, the wavelength of light can be used as a ruler.[1] Although classical displacement-measuring interferometers can be operated with high-resolution, problems do exist. These systems are usually built around bulk-optics, mirrors and beam-splitters, and for accurate fringe counting these elements need to be aligned with high precision. This is often not practical in real-world applications.

Also, ambiguities can exist in displacement directionality and when displacements exceed one wavelength. The measurement technique selected for the trial is based on fibre-delivered absolute-distance interferometry or channelled-spectral interferometry.[2, 3]

Its application to this measurement problem has clear advantages when compared to classical interferometric approaches. The technique allows a measurement of absolute distance and therefore bypasses the problems of keeping an accurate track of displacement and directionality over long timescales. A displacement measuring system would need to be continually active throughout the trial in order to maintain a datum for the measurement. Also, by using a fibre based sensor, no multi-component alignment of optics is required, making the system practical to use. In essence, the sensor system is based around four main elements, a tuneable laser source, a fibre optic gold target arrangement (forming a Fabry-Perot cavity), a detector and finally, a fibre optic circulator device which is used to direct the light signal around the sensor.

During the operation of the sensor, light from the laser is launched into the routing fibre and passed through the circulator. The light which is transmitted out of the fibre probe travels across the optical

cavity to the target from where it is scattered back towards the probe. A small portion of this reflected light (typically <1%) enters the probe and interferes with the small fraction (typically 4%) that is initially reflected from the probe end-face. As the laser frequency is varied, the modulation of the light intensity incident on the detector produces a characteristic, approximately sinusoidal, interference pattern, a shown in Figure 2. The contrast of the interference fringes can be optimised by applying thin metal coatings (typically gold) to the end face of the probe.

The fringe spacing of the interferogram, $\Delta\nu$, often called the free spectral range, can then be simply related to the distance, d, between the probe and target using equation 1.

1 $$d = \frac{c}{2n\Delta\nu}$$

where n is the refractive index of the material between the probe and target and c is the speed of light in a vacuum.

FIGURE 3

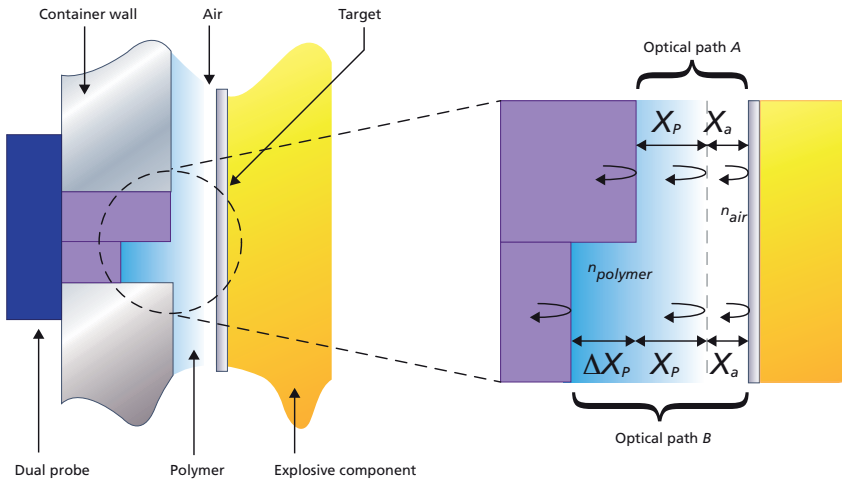

The dual probe principle for the measurement of refractive index and optical path.

The ratio between the speed of light in a vacuum and the speed of light in a material is its refractive index and is a measure of the way that light interacts with the material. At normal atmospheric pressures and temperatures the atoms and molecules in air are relatively sparse and the refractive index is close to unity. In fact n_{air}=1.0027 and in a practical sense can be assumed invariant over the temperature and pressure ranges experienced during the trial.[4] The combination of physical distance, d, and refractive index is called the optical path length (OPL). The factor of two is included to describe the round trip of the light back from the target to the probe.

2 $$OPL = 2nd$$

"The technique allows a measurement of absolute distance and therefore bypasses the problems of keeping an accurate track of displacement and directionality over long timescales."

FIGURE 4

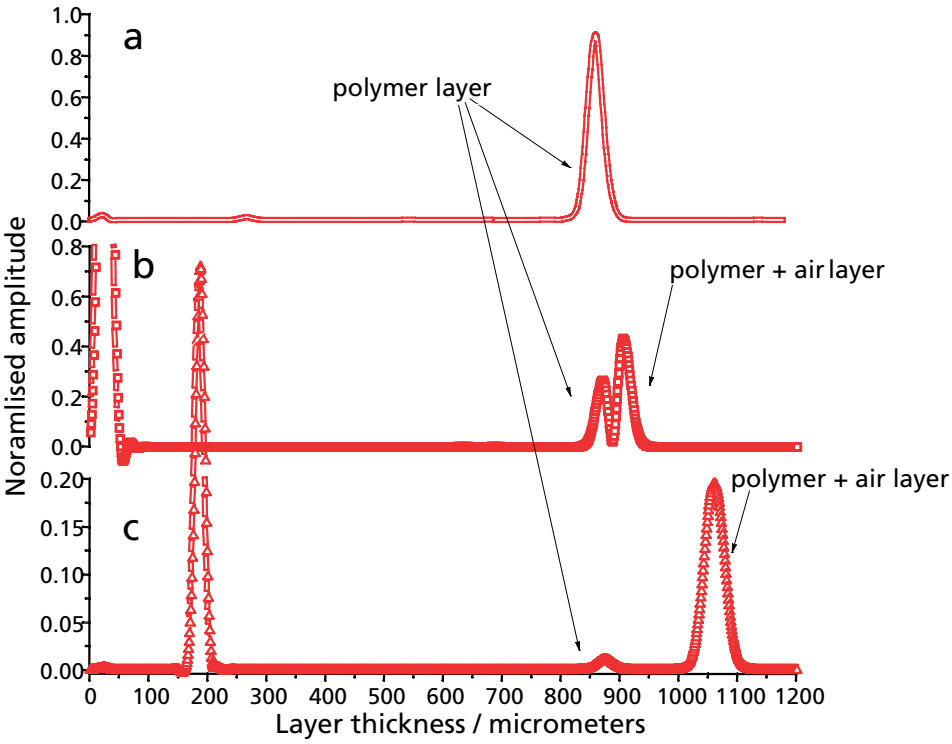

FFT data showing discrimination between polymer and air with (a) Single polymer layer present, (b) Air gap is induced and detected, (c) Air gap is increasing in thickness.

FIGURE 5

Visualisation of the probe design concept.

This means that if the FODS is used to measure the distance through air, the distance can be determined directly with the knowledge of the fringe spacing of the interference pattern. Fringe spacing can be determined using a variety of techniques. A combination of a fast Fourier transformation (FFT) algorithm and peak fitting techniques were used to extract the spectral density information, which is related to distance. The measurement of distance on a micrometre scale is extremely challenging when translating objects relative to each other. One method in which the performance of the sensor is evaluated is via

a highly rigid and stable linear reference rig, rigorously designed to minimise off-axis motion and environmentally induced measurement errors. The test arrangement was designed around a linear airbearing stage. The movement of this plate is monitored with an independent Renishaw® reference interferometer which has its wavelength traceable back to the primary national standard at the National Physical Laboratory. The sensor was evaluated over a range of 3.5 mm, far exceeding the trial requirements, demonstrating an error in the FODS system of less than ± 10 µm. The error characteristically increases with measurement distance due to a decrease in the signal to noise ratio of the interference fringes. It should be noted that this random error can be reduced with the successive averaging of measurements. This result shows that, in principle, the sensor concept is suitable for the trial.[5]

Multi-Layer Measurement Technique

As discussed, the trial sensing path length is complicated by the presence of polymer and air layers between the probe and target. A typical transparent polymer has a refractive index around 1.4 in the near-IR spectral domain, close to standard silica glass. The refractive index of the material, like glass, varies with temperature and any applied stress or strains due to the thermo-optic and photo-elastic effects. It is not practical to make direct measurements of temperature and stresses at the probe locations and therefore the refractive index of the polymer cannot be indirectly determined by the generation of calibration 'look up' sheets for known temperatures and stresses. To solve this problem a dual-probe arrangement was conceived which makes a simultaneous measurement of optical path, refractive index and hence the distance.[6] This is performed by the means of a mechanical discrimination technique, with two measurement legs with a known lateral offset, ΔXp, creating two separate optical paths through the polymer, illustrated in Figure 3. Due to their close proximity, it can be assumed that the refractive index, n_p, is the same in each measurement path. Therefore the refractive index is found by subtracting one optical path from the other and dividing by 2ΔXp, giving equation 3.

> "The measurement of distance on a micrometre scale is extremely challenging when translating objects relative to each other."

When the system encounters any additional transparent layers, the FFT routine is used to discriminate between the interference signals between each optical interface. In this case, demonstrated in Figure 4, experimentation and modelling show that multiple FFT signals are resolved corresponding to each physical layer in the system.

Initially, (as in Figure 4(a)) if a single layer system exists, a single frequency is present; with the introduction of another layer (e.g. an air pocket), a low frequency component is also detected (Figure 4(b)). To begin with, the smaller secondary layers are detected as a splitting of the single frequency into two distinct frequencies corresponding to the two separate layers. This becomes more defined in Figure 4(c) as the second layer increases in thickness.

3 $$n_p = (OPL_B - OPL_A)/(2\Delta X_P)$$

FIGURE 6

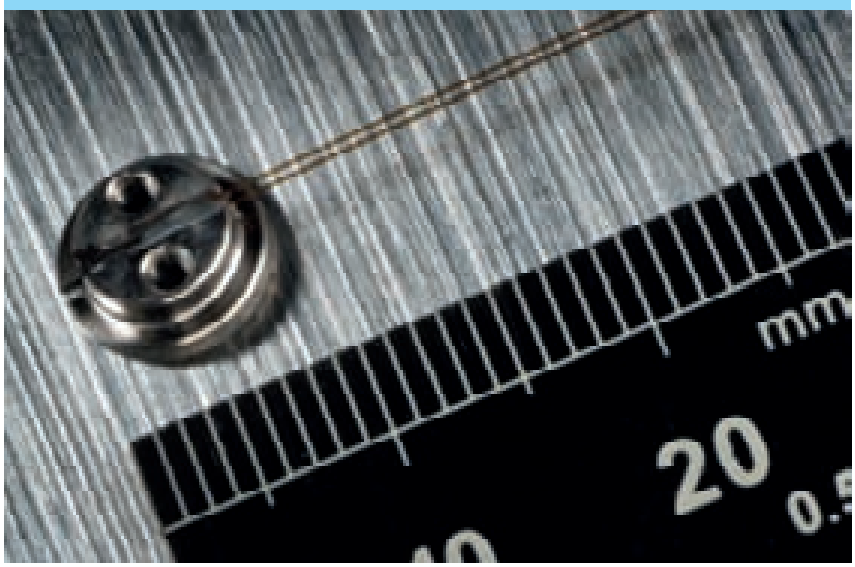

Image of the completed probe plug arrangement formed from the combination of two half blocks.

FIGURE 7

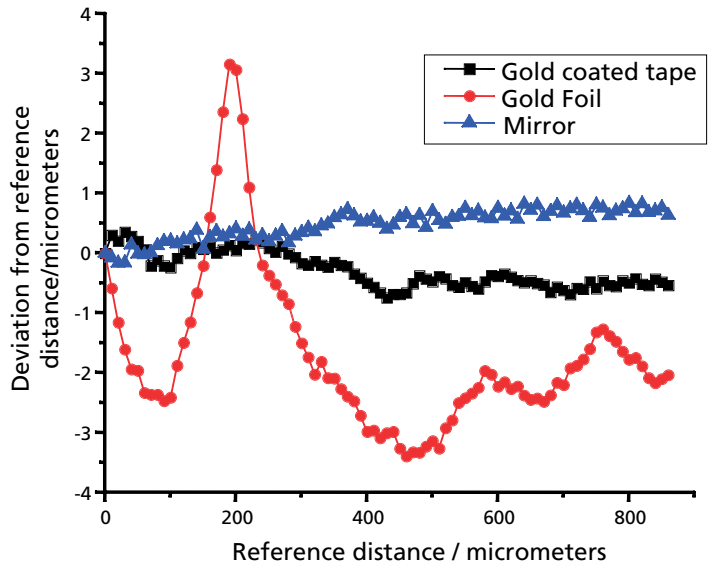

Target comparison showing data collected on the linear reference rig.

Although it is beyond the scope of this article, fibre Bragg grating based optical temperature sensors were also designed and manufactured for inclusion in the trial assembly.

Trial Transducer Development

With the FODS proof of principle demonstrated within a laboratory environment, the next step was to engineer the concept into a robust and deployable solution.[7] Engineering the concept proved to be a challenge, involving the ruggedisation of the probe-target arrangement, development of a ruggedised interrogation unit and the refinement of software control and analysis programmes.

No suitable technology was commercially available for use as a ruggedised transducer (probe-target arrangement), hence an R&D programme was embarked on. This resulted in the development of a unique optical arrangement.

The light in standard telecoms optical fibre is guided within a small central core region, which is approximately 9 μm in diameter: light in this region is referred to as being in the guided mode. This confinement or wave-guiding is usually achieved via a step refractive index change between the core and its surrounding cladding material, which is 125 μm in diameter.

When optical fibre is bent, subtle changes in the ratio of the core/cladding refractive indices cause light to couple from the core out into the cladding, with the exact losses being dependent on wavelength. This de-coupled light then leaks out of the cladding and is lost. When the bending radius is less than about 20 mm this signal loss is significant and will ultimately compromise the operation of the sensor.

The obvious option would be simply to package the fibre in a large support housing. It was decided that this level of intrusion into the host system could not be tolerated. This generated the requirement for the development of a low profile beam turning fibre optic probe. The main aim was to develop a probe which, whilst maintaining signal levels, could turn the probe beam through 90° in the smallest volume possible.

Several designs were explored, including micro prisms and angled end-face polished fibre. Although these methods were desirable in terms of size, initial experiments demonstrated poor signal levels due to low levels of light coupling back into the probe. The final solution was to combine single mode fibre for signal delivery into the test assembly with short lengths of polished fibre to provide wave-guiding closer to the target, thus increasing returned signal levels within a compact volume.

The initial design consisted of a 'lead fibre' with a core cladding ratio of 9/125, which provides single mode guiding at 1550 nm for signal delivery, butt-coupled to another fibre. This is illustrated in Figure 5 and is known as the 'probe fibre'. To prove the technique and manufacturability of this design the first generation probe fibres had a 300/330 core cladding ratio. Subsequent generations were produced until a repeatable manufacturing technique to assemble 9/125 to 9/125 was devised.

FIGURE 8

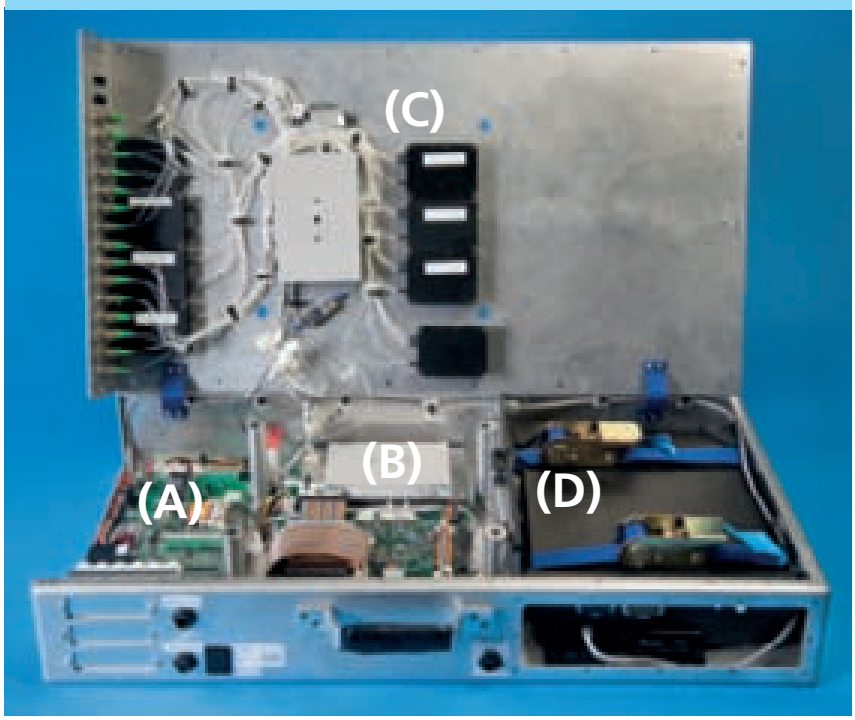

RUGINT system designed to operate under 20 gn loading

"No suitable technology was commercially available for use as a weaponised transducer (probe-target arrangement), hence an R&D programme was embarked on."

This final arrangement provides the maximum bi-directional throughput of light.

The alignment and bonding of the lead and probe fibres proved to be demanding. In essence, two fibre cores of outer diameter 9 µm were precisely aligned in free space. The alignment is achieved by active measurement of optical power throughput with the aid of an optical source and detector. Once the signal is maximised, the fibres are bonded together using a specially selected adhesive and then bonded to a metal substrate block, as illustrated in Figure 6.

The transducer is completed with the addition of a suitable target, the development of which was a key aspect of the work. Target selection affects signal return, signal to noise ratio, and ultimately the accuracy of the measurement. The optical cavity that is formed between the end face of the probe and the target is essentially a Fabry-Perot cavity and as such can operate over a range of values of finesse. Finesse is a measure of the sharpness of interference fringes. High finesse signal returns are produced by multiple reflections between highly reflecting cavity surfaces such as polished mirrors, potentially giving high precision measurement. The disadvantage is that they require precise alignment of the target surface, which is not practical in this application. For this reason it was chosen to operate within a medium to low finesse regime.

"The optical cavity that is formed between the end face of the probe and the target is essentially a Fabry-Perot cavity and as such can operate over a range of values of finesse."

FIGURE 9

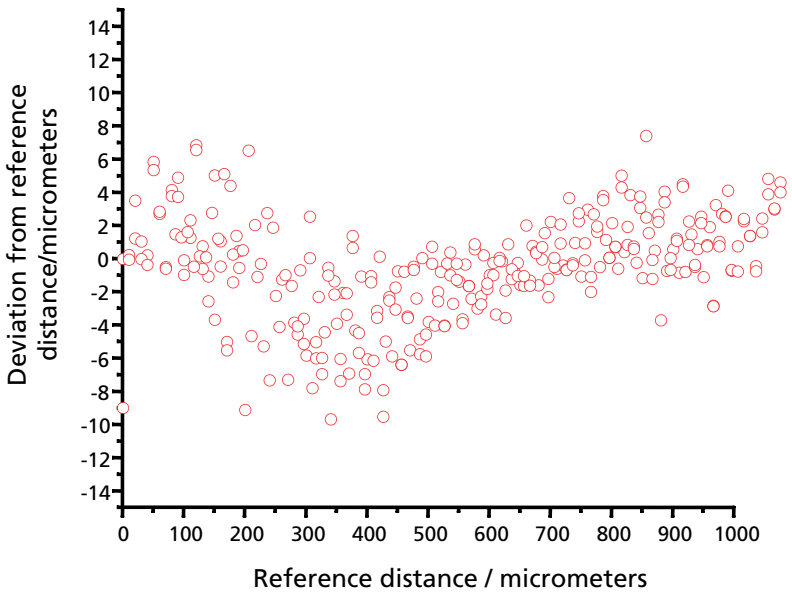

The performance of the trial sensor.

Here the signals are less sensitive to misalignments whilst still providing sufficient signal return. In Figure 7 the performances of two different target materials are compared to a reference mirror. The Goodfellows® 99.9% purity rolled gold foil produces a comparatively larger error when compared to the gold coated audio tape, the in-house developed target, and reference mirror. This is caused by the manufacturing process of the foil. The distance sensor becomes sensitive to the relatively large mean surface roughness and non-homogenous nature, which is an artefact of the rolling process.

To ensure that the optical properties of the trial targets are not spoilt during application and that application is achieved in a repeatable fashion, a tool was developed which utilises the magnetic properties of the target material. The application tool uses magnetic retention to hold the target during positioning before it is the blown on to the explosive through a release of compressed gas.

Sensor Interrogation and Data Processing

As described earlier, the sensor system was designed to operate under two different environments. During the first phase of the trial, the static thermal test, conditions are relatively benign. Here a standard network is used for instrument control, data storage and on-line analysis. During the acceleration phase, this type of infrastructure is not suitable. Historically, instrumented centrifuge tests have used slip rings for data output. However this method is not compatible with the digital signal output generated by the sensor. With no acceptable method of wireless data transmission, any instrumentation required for the sensor system must be situated on the centrifuge during the test. The closest suitable mounting point to the central axis was found to result in a 20 gn loading during a typical centrifuge cycle. Following a review of COTS technology, it was concluded that no system was available that would meet the requirements in terms of repeatability, bandwidth, channel count, power, data acquisition/ storage and self check whilst under the acceleration phase of the trial. During the concept phase, it was determined that existing commercial systems could be modified and integrated to meet the requirement.

For the optical system a modified and expanded W7 Micron-Optics® 4-channel interrogator was used as a base unit for a trial ruggedised interrogation (RUGINT) system. The W7 contains a tuning laser element operating in the communications band, around 1550 nm, along with detectors and an analogue to digital converter with a 5 Hz update rate and a 12.5 nm tuning repeatability. The W7 was modified to incorporate a 4-in/16-out solid state electro-optical switch. To expand the capacity further, each channel was split in the spectral domain into two further channels, using coarse wavelength division multiplexer (cWDM) devices. Wavelength division multiplexers are used in the telecoms industry to de-multiplex hundreds of telephone conversations that travel down one optical fibre. To meet the required trial channel count two RUGINTS are used in parallel, one either side of the central axis of the centrifuge giving a total of 64 channels. To include a self test capability one channel of each RUGINT is reserved to monitor the tuning parameters of the W7 laser during operation. This is achieved via an acetylene gas cell, which is a NIST traceable spectral reference, and a high finesse etalon, which is a stabilised Fabry-Perot cavity. These reference elements were used to qualify the RUGINT performance during development and prior to the trial. Figure 8 is an image of the RUGINT showing the main elements: (A)

"To expand the capacity further, each channel was split in the spectral domain into two further channels, using coarse wavelength division multiplexer (cWDM) devices."

base optical processing unit, (B) expansion optical switch, (C) cWDM's and (D) solid state laptop for control and data acquisition.

Although beyond the scope of this article, the sensor system has been through systematic levels of testing complexity, replicating the thermal and pressure regimes that will be seen during the trial. As an example of this validation, Figure 9 shows data from the linear reference rig for a typical trial probe and target used in combination with the RUGINT system in order to test the full sensor system.

Conclusion and Future Work.

The project has created a virtual team of multi-disciplined personnel coupled with a state of the art optics laboratory that is capable of developing high accuracy sensing solutions for trials, warhead environmental monitoring or condition monitoring. The team's methodology of investigating commercial options in the first instance, and conducting R&D only when absolutely necessary has provided AWE with a unique solution to a complex problem at relatively low technical and financial risk. The sensor system will be deployed in two future trials. During one of these, an inert assembly will demonstrate the FODS in its final form and under operational conditions.

References

1. P. Harihan, 'Optical Interferometry' Elsevier Science (2003).
2. H. Royer, 'Interferometry beyond the coherence length of the light source: the use of channelled spectral lines', Journal of Applied Optics, 12, 229-232 (1981).
3. C. Boulet, M. Hathaway,D. A. Jackson, 'Fibre optic-based absolute displacement sensor at 1550nm by means of a variant channelled spectrum signal recovery', Optics Letters, 29, 1602-1604 (2004).
4. K. P. Birch, M. J. Downs, 'An Updated Edlen Equation for the Refractive Index of Air', Metrologia, 30, 155-162 (1993).
5. Technology Management Guidance for the UK MOD Defence Acquisition Community version 1.3 Annex A
6. P. B. Harrison, R. R. J. Maier, J. S. Barton, J. D. C. Jones, S. McCulloch, G. Burnell, 'Component position measurement through polymer material with broadband absolute distance Interferometry', Measurement Science Technology, 16, 10, 2066-2071 (2005).
7. P. B. Harrison, D. Pask, T. Boon, R. R. J Maier, J. S. Barton, J. D. C. Jones, 'Large Scale Engineering Trial of Absolute Distance Interferometry', 18th International Conference on Optical Fibre Sensors, Cancun (2006).

Acknowledgements

The Authors would like to thank: Mr Tom Boon for his major contribution to the trial, Prof. Graham Peggs, Mr Andy Piper, the MET team, the Visualisation team, the trial Graduates, AOS Technology Ltd, Smart Fibres Ltd, and Duckworth & Kent (Reading) Ltd.

"Although beyond the scope of this article, the sensor system has been through systematic levels of testing complexity, replicating the thermal and pressure regimes that will be seen during the trial."

AUTHOR PROFILE

Dean pask can be contacted on e-mail: dean.pask@awe.co.uk

Dean Pask • Dean Pask graduated from Coventry University with a BEng (Hons) degree in Aerospace Technology in 2002. After a brief period at Airbus, he joined the Nuclear Physics Package Engineering Group in 2003. He is now a Senior Engineer within the Engineering, Research and Development Team where he has concentrated on developing sensor systems for tests and trials. He has built up interactions with industry, academia and the US national laboratories and has had the opportunity to attend the Los Alamos Dynamic Summer School. Here he worked on a project looking at the effect 'joints' have in relation to the modelling uncertainty of the dynamic properties of a structure. Dean is currently concluding an MSc in Explosives Ordnance Engineering from Cranfield University, Shrivenham, and is working towards achieving chartered status with the Institution of Mechanical Engineers.

AUTHOR PROFILE

Pete Harrison can be contacted on e-mail: pete.harrison@awe.co.uk

Pete Harrison • Pete obtained a PhD in physics from Heriot-Watt University in 2006 on the application of fibre optic technology in sensor systems. During this he was, amongst other things, particularly interested in fibre optic interferometry for small scale distance measurement. Whilst writing his thesis he spent a winter as a post doctoral researcher, where he carried out field trials of fibre optic pressure sensors for explosive shock wave characterisation. This was followed by a joint Heriot-Watt/ AWE technology transfer project to bring fibre optic sensing technology to AWE. Pete finally joined AWE in mid 2006 and works in the Warhead Technology Division. His main interests still lie in the development of novel sensor systems for field trials and condition monitoring applications.

AUTHOR PROFILE

Will Sweeney can be contacted on e-mail: william.sweeney@awe.co.uk

Will Sweeney • Will obtained an MEng in Engineering Science from the University of Oxford in 2005 studying hypersonic flow characteristics of scramjet intakes. After completing the AWE Graduate Programme, including a placement with the Directorate of Strategic Technologies, he joined the NPP Engineering, Research and Development Team in 2007, working on the development and qualification of fibre-optic based sensing systems. Will is currently studying for an EngD at Cranfield University.

Detection of Line Intensity Enhancement in Plasma due to Opacity

Opacity is a property of many plasmas and its study is a major research topic both at AWE[1] and elsewhere. It is expected that if an emission line in a plasma becomes optically thick by increasing the plasma size (for the same density) then the intensity ratio of that line to another transition that remains optically thin would decrease.

Indeed, the detection of such an effect is one of the standard methods of diagnosing plasma opacity. However, previously[2,3] we have shown that in certain cases the ratio would increase, due to the fact that an ion in the upper state of the transition can be pumped in the optically thick case by photons traversing the plasma at many different angles.

Line intensity enhancement is predicted to occur over a relatively narrow range of plasma column density (i.e. number density x pathlength). The exact range depends on several factors, including the plasma geometry, and ionic species and emission lines considered, but generally lies between 10^{13} and 10^{17} cm^{-2}. Such values of column density are common in some types of astrophysical plasmas, in particular the coronal regions of cool stars. (The corona is a region of hot gas surrounding a star – in the Sun it is visible during total eclipses as a corona or halo of white light, hence the name.) We therefore decided to examine the coronal spectra of such cool stars, to search for line intensity enhancements. Specifically, we analysed the Fe XVII 15.01 and 16.78 Å emission lines in a sample of cool stars observed by the XMM-Newton satellite. The 15.01 Å transition has a large f-value compared to the 16.78 Å line, and their intensity ratio I(15.01 Å)/I(16.78 Å) hence provides an excellent optically thick/thin diagnostic. Furthermore, both lines are strong and close in wavelength, making it relatively straightforward to measure their intensity ratio accurately.

The XMM-Newton spectra studied for our project were obtained with the reflection grating spectrometers RGS1 and RGS2, which provide data with a resolution of 0.025–0.040 Å over the wavelength range 5–38 Å. A total of 14 spectra for 5 stars were analysed, using the IDL-based software PINTofALE. Spectra were obtained during periods when the stars were quiescent and also flaring, i.e. undergoing mass and energy outbursts similar to the flares observed on the Sun. Details of the reduction and analysis procedures may be found in Rose et al.[4]

For most of the observations, the measured I(15.01 Å)/I(16.78 Å) intensity ratios agree with the predicted optically thin values (within the experimental errors), with one instance (for the star AB Dor) where the ratio is smaller than theory, as expected for an optically thick plasma (see Figure 1). However, for one spectrum, namely that for EV Lac obtained during its quiescent phase, the measured ratio of 2.50 ± 0.25 (1-sigma error) is much greater than the theoretical value of 1.85. This indicates enhancement in the 15.01 Å line intensity, as opposed to the normal reduction expected for an optically thick transition. The enhancement factor (R) is given simply by dividing the observed line intensity ratio I(15.01 Å)/I(16.78 Å) by the value calculated in the optically-thin coronal limit, i.e.
R = 2.50/1.85 = 1.4.

"A total of 14 spectra for 5 stars were analysed, using the IDL-based software PINTofALE. Spectra were obtained during periods when the stars were quiescent and also flaring . . ."

FIGURE 1

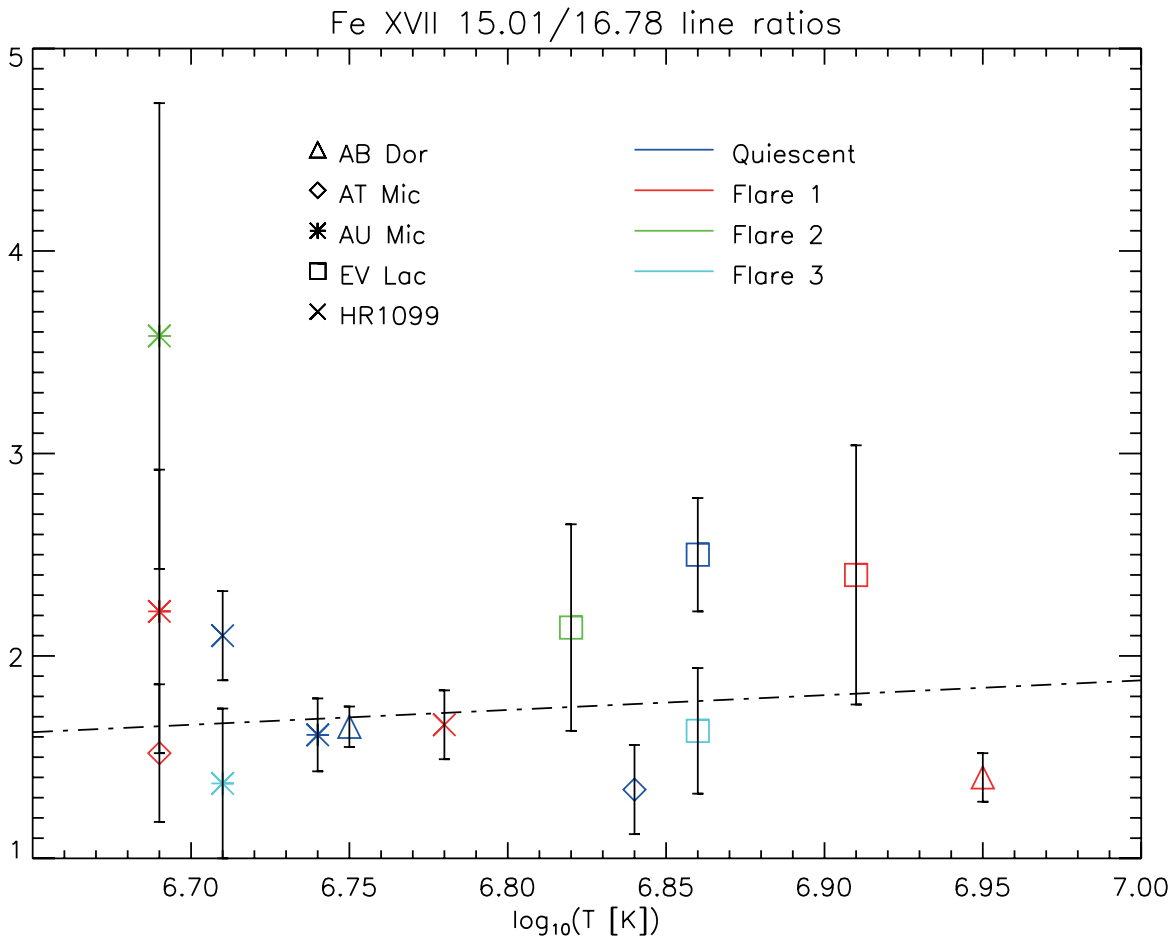

The Fe XVII emission line intensity ratio I(15.01 Å)/I(16.78 Å), obtained using the XMM-Newton satellite for a number of stars during several periods of observation (both quiescent and flare periods), where the error bars are 1-sigma. These ratios are plotted against the electron temperature (T) determined using the measured I(Fe XVIII 16.07 Å)/I(Fe XVII 16.78 Å) intensity ratio. Also shown (as a dotted line) is the predicted optically thin I(15.01 Å)/I(16.78 Å) ratio as a function of T.

Our findings are confirmed in Figure 2, which shows the spectra obtained for EV Lac during its four periods of observation. The observed spectra, and those calculated for an optically thin plasma, are markedly different only for the 15.01 Å line during the quiescent period. For the quiescent spectrum, the 16.78 Å line intensity is in good agreement with the optically thin model, whereas that for the 15.01 Å line is more intense than the model prediction.

The observed I(15.01 Å)/I(16.78 Å) line ratio being larger than the theoretical value by 2.6-sigma indicating a 99.5% confidence level of our result being a true enhancement.

The 15.01 Å line results from a 3d-2p transition, while 16.78 Å arises from a 3s-2p transition, both to the Fe XVII ground state. Consequently, as the majority of the Fe XVII ions are in the ground state, the ratio of the optical depths for the two lines is determined (to a very good approximation) by atomic physics alone, and is given by the ratio of their absorption oscillator strengths, which is 26. As the 16.78 Å line is optically thin and the 15.01 Å line is optically thick, and the ratio of optical depths is approximately 26, we conclude that the optical depth of the 15.01 Å line is, to within an order of magnitude, about 10.

FIGURE 2

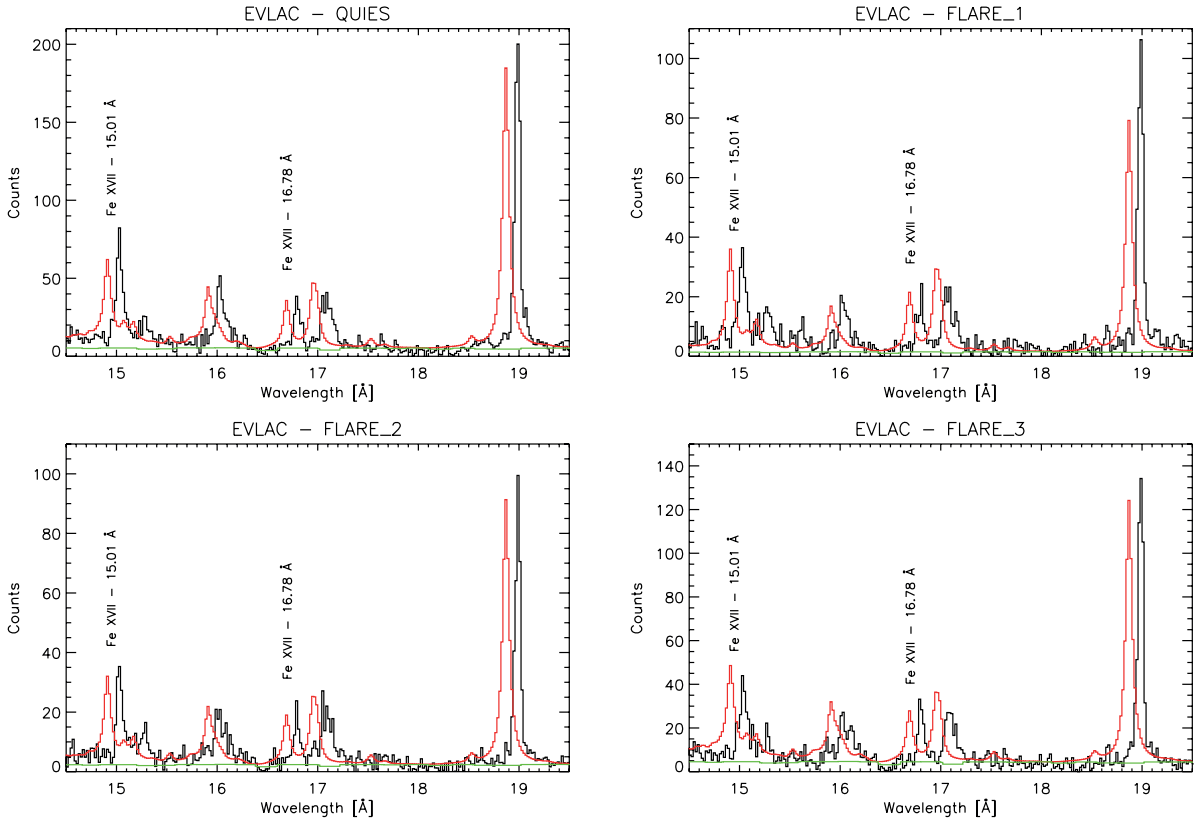

Observed XMM-Newton spectrum (red line), predicted spectrum (black line) and continuum (green line) for the star EV Lac during one quiescent and three flare periods. The wavelength grid of the predicted spectrum has been shifted by 0.1 Å for clarity. For the quiescent period only, there is a clear increase of the Fe XVII 15.01 Å line intensity, which is not observed for the 16.78 Å transition.

This conclusion can be checked by an independent calculation of the optical depth in the 15.01 Å line using plausible values for the plasma properties, including temperature (T), electron density (n_e) and plasma scale size (L). Diagnostic emission line ratios for EV Lac yield $T = 10^{6.9}$ K and $n_e = 10^{13}$ cm^{-3}, while analyses of similar coronal regions in other cool stars indicate L = 16000 km. These imply an optical depth of about 40, which confirms the order of magnitude value of 10 derived above.

Assuming that the Fe XVII emission in EV Lac arises from a plane-parallel uniform plasma, then the theoretical results of Kerr et al.[2] indicate that for an optical depth of the 15.01 Å line of 10 (in fact the dependence on optical depth is not pronounced in this range), the enhancement factor for the 15.01 Å line intensity would be R > 1 for an angle of observation to the plasma of between 0–60°, (where 0° is the perpendicular to the face of the plane-parallel plasma), and R < 1 between 60–90°. By contrast, the theory indicates that a uniform spherical plasma can have a transition of high optical depth, yet the line would have the same intensity (to a distant observer) as if it were optically thin (i.e. R = 1), because the effect of

FIGURE 3

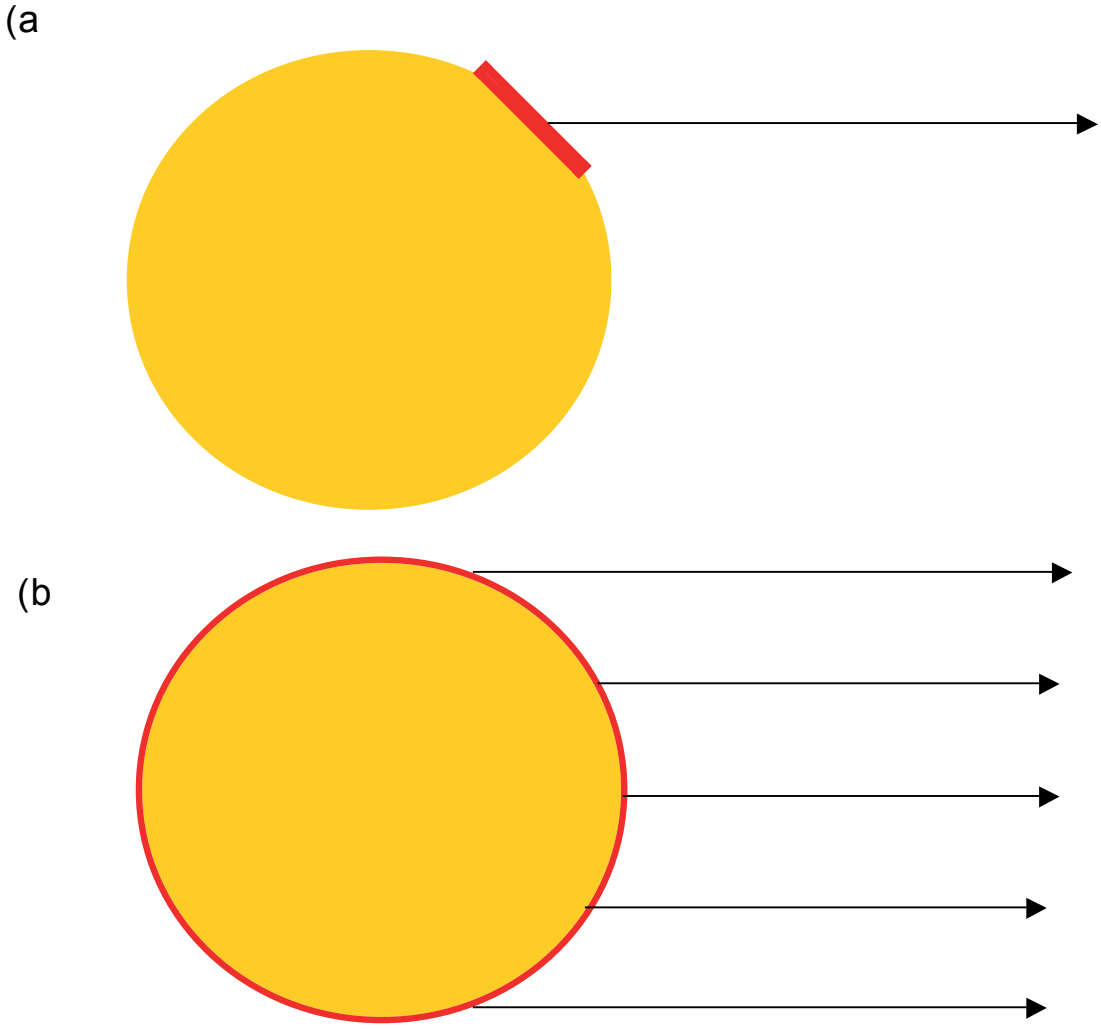

(a) A simple illustration of a plane-parallel Fe XVII emitting region on a star's surface that would appear as a plane-parallel plasma at an angle to the line-of-sight to Earth, leading to a detection of intensity enhancement in the 15.01 Å line.

(b) The larger surface coverage of the Fe XVII emission (possibly during flare periods) would lead to no net intensity enhancement (i.e. R = 1), as indeed is found for most of our XMM-Newton satellite observations in Figure 1.

pumping and depletion exactly cancel due to the unique symmetry of a sphere. The same result is found for a spherical shell of uniform plasma where the ratio of shell thickness to radius is large. This may explain why coronal opacity has proved so difficult to detect in stellar sources if emission is present over a large portion of the stellar surface.

Our measurement of an enhancement factor for the 15.01 Å line of R = 1.4 indicates that the Fe XVII emission cannot be present over most of the surface of EV Lac, as this would lead to R = 1. One possible geometry for EV Lac that would yield the present result is a plane-parallel region of Fe XVII emission taking up a fraction of the star's surface during the quiescent phase, and lying at an angle to the line-of-sight to Earth. By contrast, if the Fe XVII emission were spread over the complete stellar surface (possibly during flare periods), this will lead to R = 1, as indeed is found for most of our observations in Figure 1.

A simple diagram illustrating the geometries involved is given in Figure 3.

We can see from the above that the detection of line enhancement due to opacity potentially provides a way to derive information on the geometry of a plasma – of particular importance for distant astronomical sources (such as stars) which cannot be spatially resolved. It is therefore important to extend our work. Specifically, we need to compare our theoretical models with experimental data from plasmas of known geometries. This can be achieved in two ways. The first is to use spatially and spectrally-resolved solar observations and such data are currently being gathered using the Hinode and SOHO satellites. Secondly, one can produce a plasma of known geometry and measurable conditions within the laboratory, for which the geometrical dependence of the line ratio can be measured. A design for some preliminary experiments may be found in Rose et al.[3] We hope to report on these and other aspects of our research programme in a future issue of Discovery.

Acknowledgements

Francis Keenan is grateful to AWE Aldermaston for the award of a William Penney Fellowship. The author also recognises the contributions of fellow authors, Mihalis Mathioudakis, Steven J Rose, Justin S Wark and Marco Matranga in the preparation of this paper.

References

1 D. J. Hoarty, et.al., J. Quant. Spectrosc. Rad. Transfer, 99, 283 (2006).

2 F. M. Kerr, S. J. Rose, J. S. Wark and F. P. Keenan, Astrophys. J., 613, L181 (2004).

3 S. J. Rose, F. M. Kerr, J. S. Wark and F. P. Keenan, AWE Aldermaston Plasma Physics Department Annual Report 2005, 119 (2006).

4 S. J. Rose, M. Matranga, M. Mathioudakis, F. P. Keenan and J. S. Wark, Astron. Astrophys., 483, 887 (2008).

AUTHOR PROFILE

Francis Keenan can be contacted on e-mail: F.Keenan@qub.ac.uk

Francis Keenan • Francis graduated in physics from Queen's University Belfast (QUB) in 1979, and obtained a PhD in astrophysics at QUB in 1982, on the study of hot (B-type) stars. He then spent 4 years as a postdoctoral researcher in solar physics at QUB, and was awarded an SERC Advanced Fellowship in 1986. Following his appointment to a lectureship at QUB in 1989, Francis was promoted to reader in 1991 and a chair in 1994. He became Head of the Astrophysics and Planetary Science Research Division at QUB in 1997, and Head of School of Mathematics and Physics in 2004. Francis was appointed to a William Penney Fellowship in 2003, which was recently renewed until 2011.

The Science, Engineering and Technology Awards

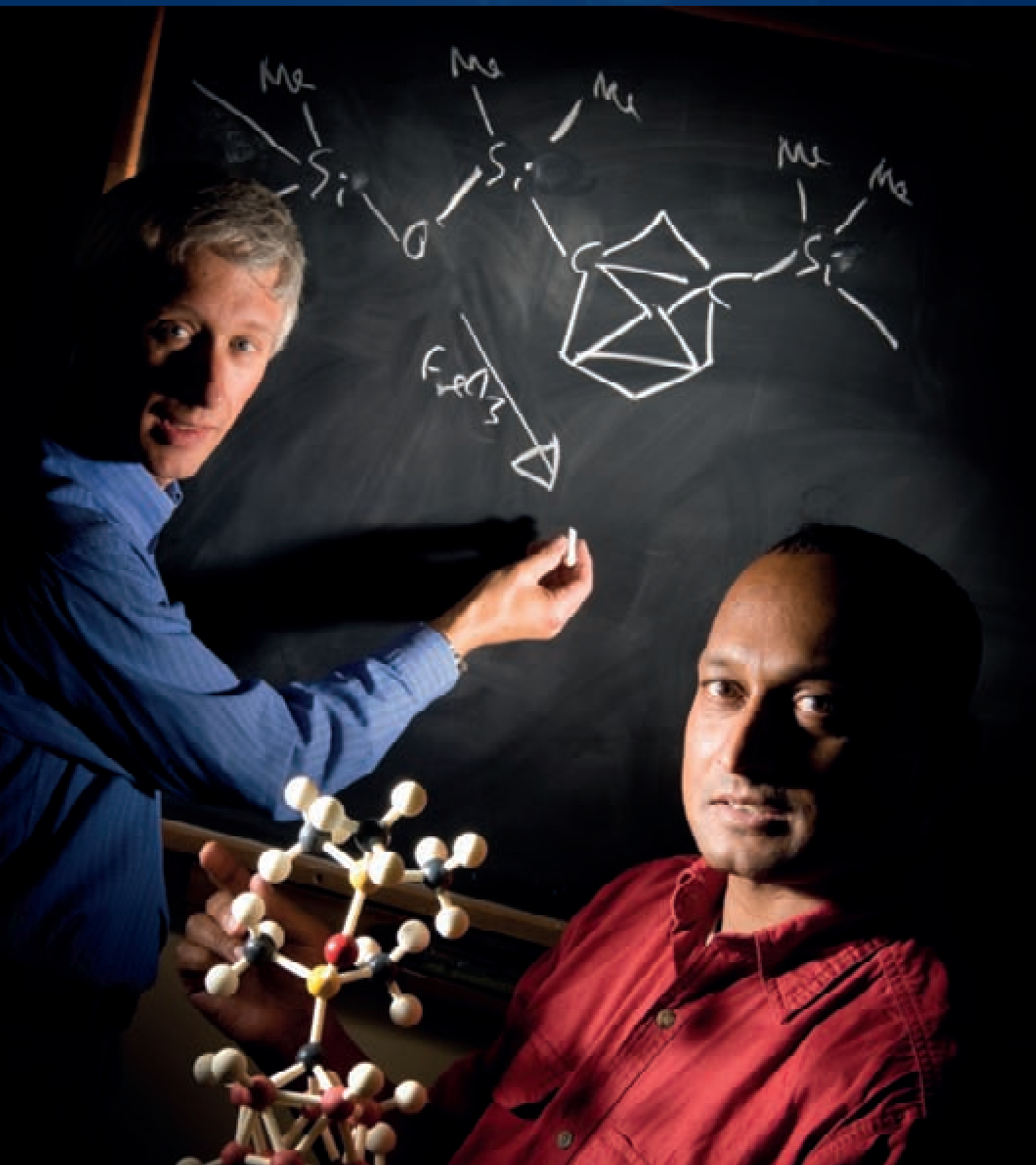

In May 2008 AWE held its fifth Science Engineering and Technology (SET) awards to honour the 2007 winners. Don Cook, AWE's Managing Director opened the event and said that AWE was one of the UK's leading centres of science, engineering and technology excellence: that reputation was built by the quality of our people and their achievements.

He commented that as in previous years judging the winners had been very difficult. The award winners were leaders in the SET field at AWE and their achievements and contributions were outstanding. This year the awards were presented by Bob McGuiness, Chief Executive of Serco Defence, Science and Technology who said he was proud on both a personal and professional level to be associated with the awards.

As in previous years there are four awards; the John Challens award is the company's most prestigious award for an individual's sustained, high quality and valued contribution to the work of AWE in the SET field; the Discovery Award is made to an individual in the early stages of their career judged to have made the most innovative and significant contribution to the SET field and demands evidence of flair and creativity; there are two J C (Charlie) Martin Awards that recognise the excellent technical content, originality and presentation in an internal and externally published paper.

THE JOHN CHALLENS MEDAL
Winner
Professor John McMordie

The John Challens Medal was awarded to Professor John McMordie, Assistant Chief Scientist. John joined AWE in 1971 after completing a PhD at the University of Wales. His main area of research during his early years at AWE was atmospheric laser propagation and damage, in particular addressing laser-induced thermal blooming and the interaction of laser radiation with materials. During this time he worked closely with the MoD conducting a wide range of operational analyses to assess the potential of high power lasers as weapons. In 1980 he took responsibility for the hardening and vulnerability programmes addressing shock loading of materials and structures and then in 1984 he moved to lead the system assessment activities. This involved supporting the MoD with battle modelling and effectiveness assessments for Chevaline and Trident as well as conducting a wide range of technical studies on nuclear deterrence issues.

In 1990 John returned to the laser area with responsibility for the AWE warhead plasma physics experimental programme using the HELEN high power laser and other high power facilities. A key activity during this time was developing the case for a successor to HELEN.

"These Company awards honour the achievements of exceptional scientists and engineers and highlight the highest levels of achievement that help make AWE a world leader in research, development and production."

In 2000, as Assistant Chief Scientist, John then took responsibility for AWE's international and university outreach programmes. A major achievement during this time has been the development of enhanced collaborations with the United States and the creation of strategic alliances with a number of prestigious universities. John is an honorary professor at Heriot-Watt University.

DISCOVERY AWARD
Winner
Peter Morrall

The 2007 Discovery Award was won by Dr Peter Morrall. Peter joined AWE just over five years ago and during this time has become a leading expert in actinide surface science. A highly innovative scientist, Peter has made significant contributions to aid our understanding of uranium corrosion behaviour and the complex chemistry of plutonium oxide surfaces.

Peter has presented work relating to the auto-reduction of plutonium oxide surface at several international meetings, and has published a paper in a peer-reviewed journal on oxide diffusion in Pu_2O_3. The diffusion coefficient for oxide ions in Pu_2O_3 was a quantity which had not previously been determined by experimental measurements. Other peer-reviewed external publications include a paper reporting the use of time-of-flight secondary ion mass spectrometry (ToF-SIMS) to probe uranium hydride corrosion sites which formed on polycrystalline uranium. This work was the first use of ToF-SIMS to study uranium corrosion, and was undertaken in collaboration with researchers at the Lawrence Livermore Laboratories in the USA. Internally to AWE, Peter has developed, and reported, a novel mathematical method to determine oxide layer thicknesses from plutonium samples under examination using X-ray diffraction. The application of this new methodology to the current X-ray diffraction analysis undertaken at AWE has given further insight into the development and transformations which occur within the oxide layers observed on plutonium.

AWARD WINNERS

From left to right: Daryl Landeg, Andy Barlow, Bob McGuiness, Clive Marsh, John McMordie, Anthony Swann, Mogon Patel, Don Cook.

Peter is highly regarded within the international scientific community and has developed close links with US laboratories, academia and other research establishments.

J C (CHARLIE) MARTIN AWARD Internal Publication

The 2006 winner of the internal publication category of the J C (Charlie) Martin Awards was an AWE Report written by Andy Barlow who works in the Design Physics Division, for a publication on "Compatible Finite Element ALE hydro" that was published at a conference at the Los Alamos National Laboratory in the USA. Andy is a regular contributor to Discovery and he explained his work in solving shock hydrodynamics problems using Arbitrary Lagrangian Eulerian hydrodynamics codes in issue four in January 2002 and also wrote about the AWE sponsored workshop on numerical methods for multi-material flow for the February 2006 issue.

J C (CHARLIE) MARTIN AWARD External Publication

For the second year in succession the winners of the external publication category of the J C (Charlie) Martin awards were Mogon Patel and Anthony Swain for their chapter on "Polymers Incorporating Icosahedral Closo-Dicarbaborane Units" which was published by Wiley-Interscience in "Macromolecules Containing Metal and Metal-Like Elements", volume 8 (2007). The book captures contributions from leading scientists within the fields represented.

"Andy is a regular contributor to Discovery and he explained his work in solving shock hydrodynamics problems using Arbitrary Lagrangian Eulerian hydrodynamics codes in issue four in January 2002"

The AWE authors currently work within the Non-Metallic Materials Research team in the Research and Applied Science directorate. AWE's achievements within this field are well recognised, and this book chapter was produced in response to a prestigious invitation to AWE from Professor Charles U. Pittman representing the American Chemical Society.

The publication communicates the chemistry and properties of boron containing polymers since the first materials were synthesised by Stock about eighty years ago. The emphasis for the development work involves boron's ability for delocalising electrons due to the presence of an empty p-orbital. The driving force to produce polymers is boron's ability to capture neutrons, release a relatively significant amount of energy on oxidation and its ability to form protective coatings.

AWE's contribution details the general synthesis chemistry and material properties of some important polymer systems incorporating icosahedral closo-dicarbaborane cages. The route toward truly multifunctional material system based around the incorporation of meta-carborane cages into polymer chains is detailed. These cage units impart enhanced thermal and chemical stability, and provide physics (neutron attenuation) and energy release properties on rupture of the caged unit. These properties have been exploited by researchers in the development of rocket fuel burn rate modifiers and within the medical field for boron neutron capture therapy.

The publication gives supportive and historical developments that allow researchers unfamiliar with the subject matter to appreciate and understand the underlying science. It should provide a useful reference for AWE scientists as well as external scientists who wish to explore this challenging and novel area of chemistry.

Neutron Spectrometry in the AWE Workplace

Since their discovery by James Chadwick in 1932, neutrons have played a crucial role in nuclear physics. Famously, neutrons provide the key ingredient for nuclear fission: when neutrons are absorbed by fissionable isotopes such as ^{235}U or ^{239}Pu, the resulting nucleus becomes unstable, and splits in two, releasing energy and more neutrons, the latter of which can be used to produce a fission chain reaction.

Neutrons are also produced as a by-product of nuclear fusion, and the energy of these neutrons may potentially be harvested in future civilian fusion-power projects.

Neutrons constitute ionising radiation and therefore provide a hazard to human health in nuclear power stations and nuclear establishments. As a consequence, the detection of neutrons is of prime importance to neutron protection and dosimetry. Neutrons have no electrical charge and are therefore difficult to detect because they cannot interact directly with the bound electrons in a material to cause their ionisation or excitation. Neutrons can, however, be detected by their interactions with the nuclei of atoms, which can take three forms: elastic scattering, inelastic scattering, and absorption (see Box 1).

It is a feature of elastic neutron scattering that the smaller the mass of the target nucleus, the greater is the amount of energy that the neutron can transfer to the target. If the energy transfer is sufficient, the target atom will be torn free of some of its electrons, and will begin travelling through the medium in which it was embedded as a positively charged ion, creating a track of further ionisation in the medium. An atom with a large atomic number (the Z number) will suffer little recoil when a neutron impinges upon it, rather like a ping-pong ball hitting a bowling ball. Hence, neutrons transfer little energy in elastic scattering interactions with large-Z nuclei. In contrast, the energy transfer is high when a neutron strikes a low-Z nucleus. In particular, when a neutron strikes the nucleus of a hydrogen atom, (which consists of a single proton), the interaction is akin to one snooker ball striking another and all of the neutron's energy can be transferred to the proton. This reduction of neutron energy provided by an intervening medium is referred to as neutron moderation. Inelastic neutron scattering is highest for high-Z nuclei, but results in less energy transfer than the elastic scattering provided by low-Z nuclei. Hence low-Z materials are generally used for neutron moderation. Neutron absorption requires neutrons to be slowed down to low energies, but is not dependent in any regular fashion on the Z-number: nuclei receptive to absorbing neutrons are distributed at various Z-numbers.

There are several processes at AWE that potentially subject the worker to a neutron radiation dose. These exposures arise mainly from fissionable material processed within glove boxes. The neutron dose is dependent on the neutron energy spectrum, i.e. the distribution in speed of the neutrons. The range of neutron energies in the AWE workplace is enormous, covering nine orders of magnitude. Neutrons in thermodynamic equilibrium with their surroundings are referred

Box 1

Elastic scattering is a collision process in which the outgoing particles are the same as the incoming particles and the total kinetic energy of the particles before the collision is the same as the total kinetic energy of the particles after the collision. In contrast, interactions in which the outgoing particles are the same as the incoming particles, but the kinetic energy is not conserved, constitute inelastic scattering. Inelastic neutron scattering occurs when the incoming neutron interacts with the nucleus of an atom and some of the energy from the incoming neutron raises the nucleus to an excited energy state. When an incoming neutron is absorbed by a nucleus, it also raises the nucleus into an excited energy state. The excited nuclei produced by inelastic neutron scattering and absorption then subsequently decay, with the release of various decay products.

FIGURE 1

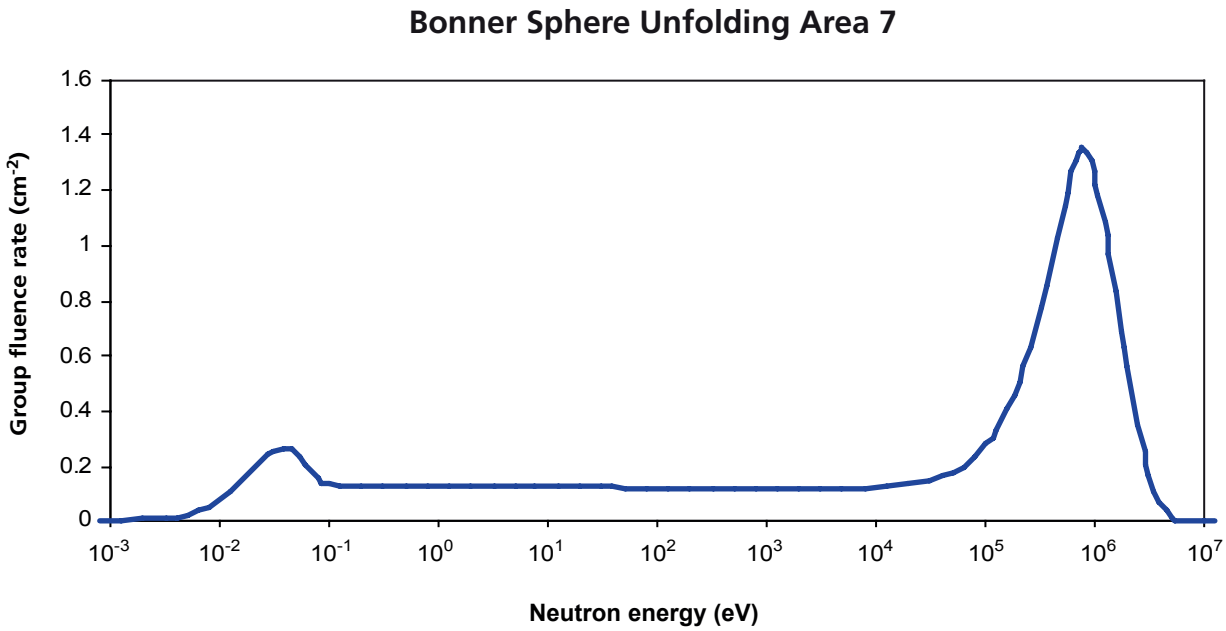

Figure 1a: area 7 spectrum, representative field. The thermal peak is relatively small and the high energy peak is much larger with a 'classic' flat 1/E energy distribution in the intermediate energy region.

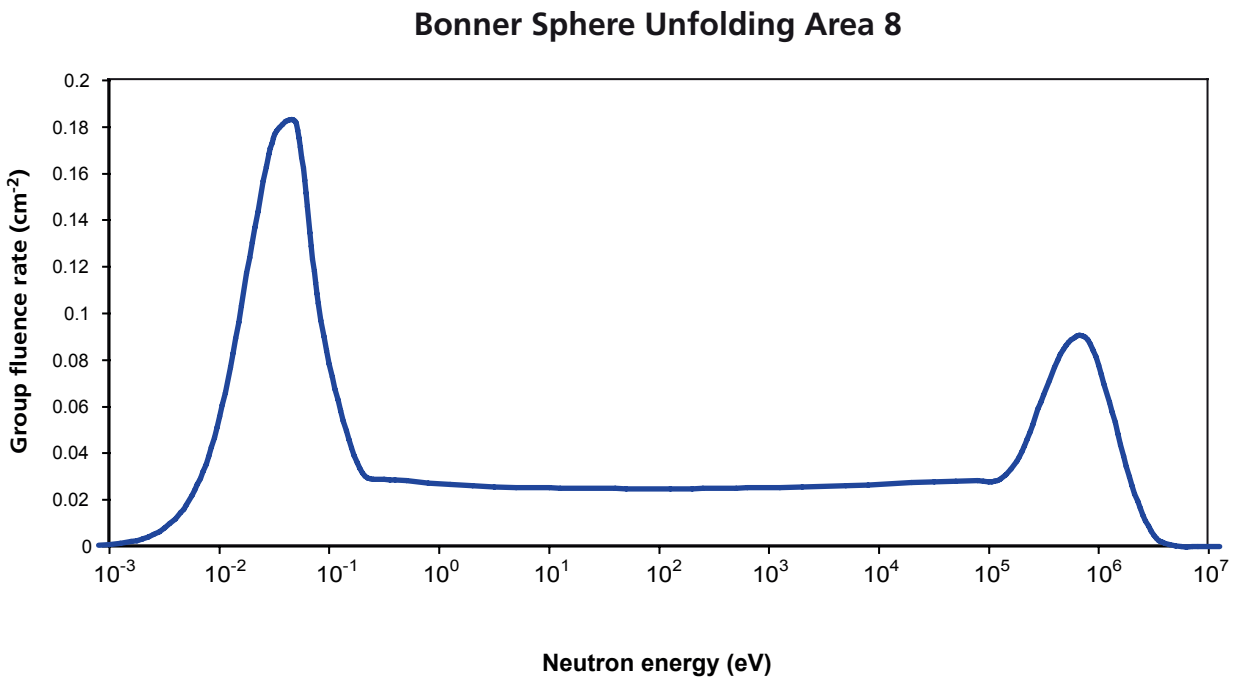

Figure 1b: area 8 spectrum (2nd example). The thermal component is significantly larger than the high energy component.

to as 'thermal' neutrons and at a room temperature of 20°C possess a peak energy of 0.0253 eV, and travel at about 2,200 m s^{-1}. The neutrons released in fission processes have a range of energies from about 1 eV to 10 MeV, whilst the neutrons released in a deuterium-tritium fusion reaction have an energy of 14.1 MeV, and travel at about 0.17 the speed of light (50,000,000 m s^{-1}). However, the neutron spectrum to which workers are exposed will be transformed by the moderation and shielding between the neutron source and the worker. The moderator consists of a low-Z hydrogenous material, such as water, carbon, flesh and plastics, in which elastic neutron scattering lowers the neutron energies and the moderator then absorbs the low energy neutrons. The shielding will typically consist of a high-Z metal, that provides protection from the gamma radiation which accompanies a neutron source, and from any secondary radiation emitted by nuclei in the moderator that have absorbed neutrons. Typical workplace neutron spectra are shown in Figure 1.

FIGURE 2

In this article we will consider the characteristics of the Harwell 95/0949 neutron dose-rate monitor, the motives and results of using Bonner-sphere spectrometry to characterise AWE's workplace neutron fields, the difficulties of unfolding neutron spectra from Bonner-sphere measurements, the solutions employed for such unfolding, and future developments.

The Harwell 95/0949 Neutron Dose Rate Monitor

The most common instrument for measuring neutron dose rates in the AWE workplace is the Harwell 95/0949, shown in Figure 2. The instrument is designed to measure a quantity $H^*(d)$, with d =10 mm, called the ambient dose equivalent (ADE), which is the operational quantity recommended by the International Commission on Radiation Units and

"The moderator consists of a low-Z hydrogenous material, such as water, carbon, flesh and plastics, in which elastic neutron scattering lowers the neutron energies and the moderator then absorbs the low energy neutrons"

Box 2

From the International Commission on Radiation Units and Measurements.[3]

The ambient dose equivalent H*(d) at a point in a radiation field is the dose equivalent that would be produced by the corresponding expanded and aligned field in the ICRU sphere at a depth d on the radius opposing the direction of the aligned field. The ICRU sphere is a spherical, tissue equivalent phantom, 30cm in diameter. The expanded radiation field is obtained by taking the fluence, energy distribution and directional distribution of the field at the point of interest and defining those values to be the values of a homogeneous radiation field over a volume sufficiently large to encompass the spherical phantom. The aligned field is one in which the radiation is oriented in only one direction.

Note: The unit of ambient dose equivalent is joules per kilogram ($J.kg^{-1}$).

The ICRU sphere model is used to define operational quantities for area monitoring. It comprises a 30 cm diameter tissue equivalent sphere of density 1 gcm^{-3} and a mass composition of 76.2% oxygen, 11.1% carbon 10.1% hydrogen and 2.6% nitrogen.

FIGURE 3

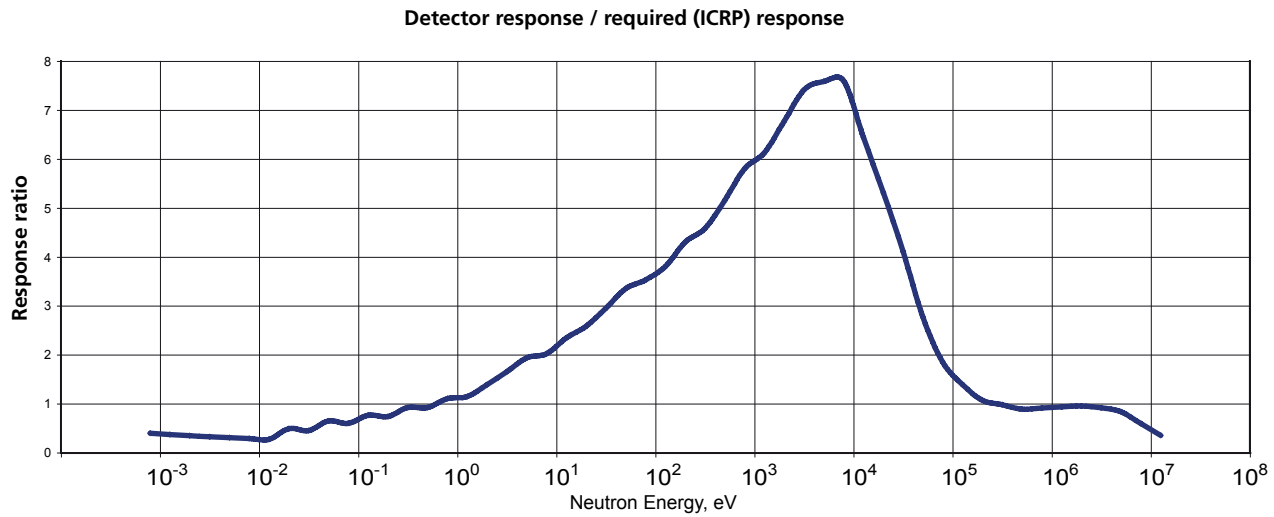

FIGURE 4

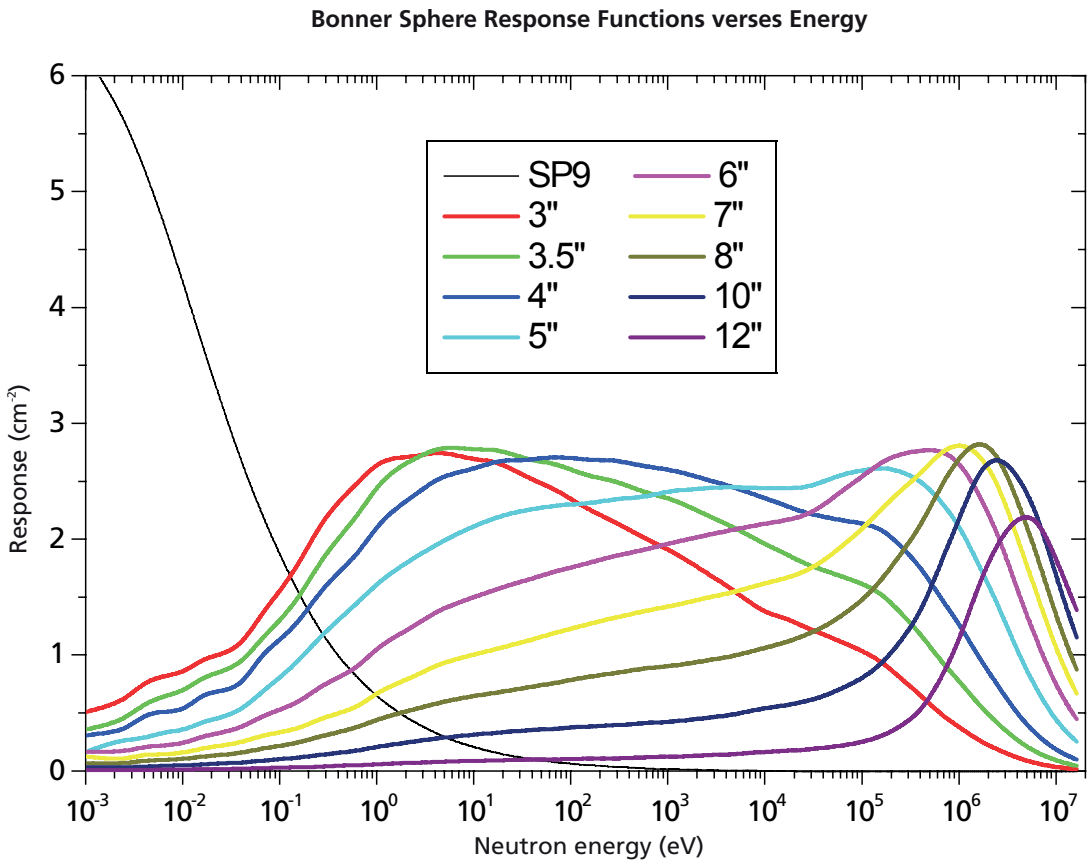

• determined by Monte Carlo techniques and monoenergetic source irradiations

Measurements (ICRU) for the area monitoring of strongly penetrating radiation, (see Box 2). The response of the instrument, however, is not ideal. Figure 3 shows a graph of the instrument (response/required response) for a range of neutron energies from thermal energies (0.025 eV) to ~20 MeV. The instrument reads almost correctly in the 1 MeV region and at ~1 eV, but over-responds in the intermediate energy region by as much as a factor of 7: it also under-responds in the thermal region and at 14 MeV by a factor of 2. Fortunately, neutron spectra typical of shielded fission sources cover a broad range of energies, and the averaged response does not deviate by more than ± 40% for a wide range of spectra.[1]

Bonner Sphere Neutron Spectrometry

To measure neutron doses more accurately requires knowledge of the neutron energy spectrum, i.e. the intensity of the neutron field with respect to neutron energy. Various neutron spectrometry systems exist commercially, but the most extensively used is the multisphere technique known as Bonner Sphere (BS) spectrometry.[2]

The BS spectrometer consists of a thermal neutron sensor, which is used at the centre of a number of different diameter polythene moderator spheres. Polythene is a low-Z material, consisting of chains of carbon and hydrogen units, in which neutrons lose their energy by means of multiple elastic scattering interactions. A certain fraction of the neutrons become thermalised by means of these interactions. The AWE set has nine spheres (of diameter 3″, 3.5″, 4″, 5″, 6″, 7″, 8″, 10″ and

Box 3

Mathematical Details of Unfolding

The general problem of unfolding a radiation spectrum requires a solution of a Fredholm integral equation of the first kind:

$$A_i = \int_0^\infty R_i(E)\Phi(E)dE$$

The task is to infer the radiation fluence Φ(E) as a function of the energy E, given a knowledge of the count-rates A_i from detector 'channels' and given the detector channel response $R_i(E)$ over the energy range. In mathematical terms, the response function $R_i(E)$ is the kernel of the integral operator.

In practice, the energy range will be divided into N discrete intervals, and one obtains a discretised version of the Fredholm equation as a matrix equation,

$$A = R\,\Phi\,,$$

in which A is a column vector with M components, Φ is a column vector with N components, and R is an M × N matrix. In explicit component terms, for the case where the Bonner spheres provide the M detector channels, one obtains:

$$A_i = \sum_{j=1}^{n} R_{ij}\Phi_j \qquad \text{for } i = 1,\ldots,\mathrm{M}$$

where:
A_i is the measured response for sphere i.
Φ_j is the fluence in energy group j.
R_{ij} is the response function of sphere i for energy group j.

The problem is to find values of Φ_j which reproduce the measured count rates A_i. However, when the number of detector channels is smaller than the number of energy groups, M < N, these equations are mathematically underdetermined, i.e., there is more than one solution to the equations.

The problem which unfolding programs attempt to solve is to minimise the χ^2 defined by:

$$\chi^2 = \sum_{i=1}^{M} \frac{(A_i - C_i)^2}{\sigma_i^2}$$

where:
M is the number of spheres
A_i is the measured response for sphere i,
C_i is the response calculated for sphere i from the unfolded spectrum
$\sigma_i 2$ is the uncertainty in $(A_i - C_i)$

Different programs use different approaches to minimising χ^2, but in the majority the unfolding leads to an iterative, trial and error approach.

The best choice of an a priori spectrum was one consisting of a thermal neutron peak, a high energy peak, and a 1/E contribution in the intermediate energy region between the two peaks. For a high energy neutron source surrounded by a good moderating material the energy distribution in the intermediate region has a 1/E dependence, i.e. it is flat when plotted on a logarithmic scale.

The thermal peak had a Maxwellian shape,

$$\phi(E) \propto \left(\frac{E}{T_1^2}\right) e^{(-E/T_1)}$$

where T_1 is the energy of the peak in the distribution, which for room temperature (20 °C) is 0.0253 eV.

The high energy peak had the shape of a fission spectrum

$$\phi(E) \propto \sqrt{E}\,e^{-(E/T_2)}$$

for a ^{235}U fission spectrum, the energy T_2 is 1.29 MeV

"The derivation of a neutron energy spectrum from measured BS responses requires the use of an 'unfolding' code. The process is, however, far from straightforward."

12″), and uses the Centronics SP9 spherical ^{3}He proportional counter as the thermal neutron sensor. The combined system of thermal sensor plus moderating spheres has a sensitivity to neutrons over a broad energy range. The sensitivity for each sphere peaks at a particular neutron energy, depending on the sphere diameter. Using the measurements obtained from a set of such spheres, information can be derived about the spectrum of the neutron field. The derivation of this spectral information, however, is not simple.

For a small sphere the degree of moderation is small, as is the capture of thermal neutrons in the moderator. Low energy neutrons thus have a reasonable probability of arriving at the thermal sensor and being detected, whereas fast neutrons tend to escape. For larger spheres there is also more capture, which means low energy neutrons tend to get absorbed in the polythene. It is the high energy neutrons which thus have the greatest probability of being detected in the sensor, and the response function peaks in the high energy region, as illustrated in Figure 4. The response functions for a range of different sphere sizes show how the peak in the response function moves to higher energies as the sphere size increases.

The AWE BS system was commissioned by collecting count data from nine different workplace areas at AWE Aldermaston during the summer of 2004. Each sphere was positioned, in turn, at a point where the neutron spectrum needed to be determined, and the count rate from the thermal sensor was recorded.

The response functions for the AWE BS set were transferred from a similar National Physical Laboratory (NPL) BS set. The response function matrix of the NPL set has been derived and refined over a number of years using the ANISN and MCNP radiation transport codes and monoenergetic neutron source irradiations at selected energies. It is very important that the response function for each sphere is known accurately, as the mathematics of the process used to extract the energy spectrum from the measurement results and response function matrix is generally very sensitive to inaccuracies and errors.

The derivation of a neutron energy spectrum from measured BS responses requires the use of an 'unfolding' code. The process is, however, far from straightforward. The underlying mathematical problem is underdetermined (see Box 3), and because of this the unfolding process requires a high level of interaction and expertise from the user.

The unfolding of the AWE BS measurements was initially performed at the NPL under contract by Dr David Thomas, an acknowledged UK expert in BS spectrometry. The principal unfolding code used in this work was the least-squares code STAY'SL, one of the new generation of unfolding codes that make the problem mathematically soluble by requiring an a priori spectrum, which is 'adjusted' on the basis of the measured count rates. NPL has considerable experience of using STAY'SL, and the code is known to produce sound results.

The NPL unfolded spectra for the nine workplace areas have certain similarities, in that they all contain a high energy peak, a thermal peak, and an intermediate energy contribution which generally approximates to a flat line when plotted on a logarithmic scale. However, there are significant differences between the nine spectra. The total neutron fluence across the different workplace areas varies from about 3 cm^{-2} to 70 cm^{-2}, and while in some cases the high energy peak is larger than the thermal peak, in other workplace areas the opposite is true. The intermediate energy contributions also vary in height, and can slope in either direction. Figure 1 shows example spectra from two different areas.

The Analytical Sciences (ASc) group at AWE now routinely use an unfolding code called MAXED, from the UMG package of codes provided by the German standards laboratory PTB. An analysis using MAXED applied to the nine areas provided an independent estimation to the NPL unfolded spectra. The starting (default) spectrum was carefully chosen and was selected to be the same for all nine areas.

FIGURE 5

The results of the two different codes were found to be in reasonable agreement.

As a further development, two unfolding codes have been developed by the ASc group at AWE which run on Microsoft Excel. These were specifically designed for the general form of the AWE neutron spectrum. The control panel for these codes is very user friendly and intuitive. Various spectrum parameters can be adjusted independently by altering corresponding slider positions, and the computed spectrum, as well as the goodness of fit between the actual and theoretically predicted count rates, are displayed in real-time, thus allowing the user instant feedback for refined adjustments. The codes calculate the fluence and ADE rates, as well as the ADE rate that would be displayed on a 95/0949 neutron monitor if placed at the measurement location.

Results from the in-house codes for the nine areas and a few later additional area measurements, show that, in general, the 95/0949 dose-rate monitor over-reads by approximately 10%, the error being on the 'safe side' of a dose-rate measurement.
Variation between the different areas is small in terms of an area survey instrument measurement (within ±10%), so specific area correction factors are not required.

The ASc group have now had over two years of experience in using MCNP5 and using and developing unfolding codes for a variety of applications. From the experience gained with guidance from NPL, we are now able to independently determine our own response functions and confidently unfold the results of future BS measurements.

"The Analytical Sciences (ASc) group at AWE now routinely use an unfolding code called MAXED, from the UMG package of codes provided by the German standards laboratory PTB."

"In order to type test and evaluate personal neutron dosimeters, a controlled, reproducible and well characterised neutron field is essential."

Representative Workplace Field at AWE

In order to type test and evaluate personal neutron dosimeters, a controlled, reproducible and well characterised neutron field is essential. Therefore to replicate a representative AWE workplace neutron spectrum, a moderator consisting of boron-loaded polythene and steel was designed and constructed around a ^{252}Cf source in the AWE neutron irradiation facility. (Californium-252 undergoes spontaneous fission, and releases neutrons in the process.) Figure 1a shows a typical workplace spectrum at AWE. A detailed MCNP5 computer simulation of the system was developed to determine the precise effect of the moderator, and the calculated neutron spectrum was confirmed by experimental measurement using Bonner sphere spectrometry.

Figure 5 shows the moderator assembly, mounted on an aluminium tube tripod directly above the neutron source carousel (background) in the neutron irradiation facility. Also shown is a 5″ Bonner Sphere spectrometer in front of the moderator, supported by a low scatter aluminium tripod system. The system is capable of generating dose rates in the range of 1 – 100 μSv per hour at a distance of 1 metre.

It is envisaged that different source/moderator assemblies will be designed to replicate variations in the AWE workplace field and to represent the neutron fields typical of other establishments. Owing to the modular design of the system this flexibility can be achieved by simply exchanging the moderator fitted on the top of the tripod support system.

Future Developments – Gold Foil Activation BS Spectrometer

In principle any thermal neutron detecting device can be used as the central sensor of a BS system. For example, materials such as gold or indium, which become radioactive following the absorption of thermal neutrons, can be used as such sensors.

Thus an extension to the existing Bonner sphere system, based on activation of gold foils is currently under development. The gold sensor is activated by deployment in the neutron field and then subsequently measured for gamma activity. Naturally occurring gold is 100% gold-197. When a gold-197 nucleus absorbs a neutron to become gold-198, it decays in accordance with a very simple decay scheme (see Figure 6). The gold-198 decays to mercury-198 by emitting a beta particle, followed by a distinct 412 keV gamma photon. Gold has stable chemistry, a well known metallurgy, and a very convenient half life of approximately 2.7 days, so that irradiation times can be practical while still allowing a reasonable time to transport the foils to the laboratory for analysis.

"The ASc group have now had over two years of experience in using MCNP5 and using and developing unfolding codes for a variety of applications."

This system has several advantages:-

- It can be used in both constant and pulsed neutron fields where an 'active' detector (employing real-time electronics) would become saturated, leading to dead time issues.
- It requires no electrical connections and is thus highly portable and can be set up quickly, making it very useful in hazardous or high dose environments, such as those containing explosives or nuclear reactors.
- It can be used in areas where there is a risk of physical contamination, since the Bonner spheres can be placed inside a protective layer, such as a plastic bag, which is relatively easy to dispose of without the spheres themselves becoming contaminated.
- The system is largely insensitive to photons and can therefore be used in mixed fields with a high gamma component, such as the accelerators used in medical radiology. It does, however, suffer from lower sensitivity and poorer resolution than active systems.

An important difference between passive and active systems is that, by definition, active systems take measurements at the time of irradiation, while passive systems such as the foil set need to be removed after irradiation, and separately analysed. Corrections need to be applied to take into account the radioactive decay which occurs during transport to the lab, and during the analysis itself.

The activity of the irradiated gold foil can be deduced either by beta proportional counting, which is the method used by NPL, or by gamma spectrometry. The intention at AWE is to use a high purity germanium gamma spectrometer to measure the activity. This method is highly

FIGURE 6

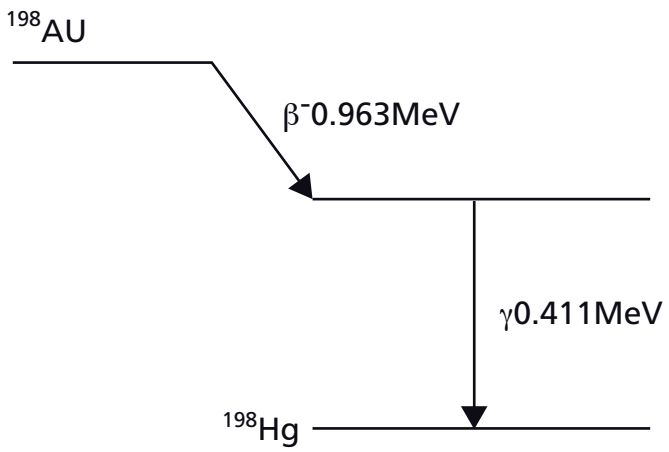

Decay Scheme of ^{198}AU

suitable because of the distinct 412 keV gamma emission by the gold foil, and by virtue of the fact that thicker foils can be used for gamma analysis; the beta electrons have lower penetration, and would be absorbed by the thicker foils before they reached the detector.

Acknowledgments

The contribution of David Fletcher, of the Analytical Sciences group AWE(A) is recognised for his input on 'Future Developments-Gold Foil Activation BS Spectrometer'.

References

1. G.F. Knoll, Radiation detection and measurement, Wiley,(1979).

2. D.J. Thomas and A.V. Alevra, "Bonner sphere spectrometers – a critical review" Nuclear Instruments and Methods in Physics Research A 12-20, 476, 1-2 (January 2002).

3. Conversion coefficients for use in radiological protection against external radiation ICRU Report 57. (1 August 1998).

AUTHOR PROFILE

Peter Danyluk can be contacted on e-mail: peter.danyluk@awe.co.uk

Peter Danyluk • Peter obtained a BSc in physics at Reading University in 1978. He joined the Safety Division at AWE in 1980 where he worked on improving the phoswich X and gamma ray detection system used at the whole body monitor for measuring plutonium in the lung. He later developed a number of analytical techniques for the calibration of radiological instruments. In 2007 he joined the solutions team in the analytical sciences group and is currently involved in the development of neutron spectrometry techniques.

AUTHOR PROFILE

Gordon McCabe can be contacted on e-mail: gordon.mccabe@awe.co.uk

Gordon McCabe • Gordon obtained a philosophy of physics PhD in 2000 from the University of Reading. After publishing papers on the mathematical structure of general relativistic cosmology and quantum cosmology, Gordon wrote a book on particle physics, 'The Structure and Interpretation of the Standard Model', published by Elsevier in 2007. he joined AWE's dosimetry service the same year, and has been working on nuclear test veteran issues, and the use of statistics and uncertainty within Analytical Sciences (ASc).

Discovery

Find out more about AWE at our website:

www.awe.co.uk

For further copies of this journal and details of other AWE publications, please write to:

Corporate Communications Office
Building F6.1
AWE Aldermaston
Reading
Berkshire
RG7 4PR